

RECORD
2022/11

PORTABLE XRF ANALYSIS IN THE JOE LORD AND PERTH CORE LIBRARIES – METHODOLOGY AND CASE STUDIES

MJ Wawryk and EA Hancock



Government of Western Australia
Department of Mines, Industry Regulation
and Safety

Geological Survey of
Western Australia





Government of **Western Australia**
Department of **Mines, Industry Regulation
and Safety**

RECORD 2022/11

PORTABLE XRF ANALYSIS IN THE JOE LORD AND PERTH CORE LIBRARIES – METHODOLOGY AND CASE STUDIES

MJ Wawryk and EA Hancock

PERTH 2022



**Geological Survey of
Western Australia**

MINISTER FOR MINES AND PETROLEUM
Hon Bill Johnston MLA

DIRECTOR GENERAL, DEPARTMENT OF MINES, INDUSTRY REGULATION AND SAFETY
Richard Sellers

EXECUTIVE DIRECTOR, GEOLOGICAL SURVEY AND RESOURCE STRATEGY
Jeff Haworth

REFERENCE

The recommended reference for this publication is:

Wawryk, MJ and Hancock, EA 2022, Portable XRF analysis in the Joe Lord and Perth Core Libraries – methodology and case studies: Geological Survey of Western Australia, Record 2022/11, 39p.

ISBN 978-1-74168-975-4

ISSN 2204-4345

Grid references in this publication refer to the Geocentric Datum of Australia 1994 (GDA94). Locations mentioned in the text are referenced using Map Grid Australia (MGA) coordinates, Zones **50** and **51**. All locations are quoted to at least the nearest 100 m.



External X-ray fluorescence analyses and assays were conducted with the Minalyzer CS and PANalytical MagiX FAST XRF instruments at the Australian Resources Research Centre (CSIRO).

Disclaimer

This product uses information from various sources. The Department of Mines, Industry Regulation and Safety (DMIRS) and the State cannot guarantee the accuracy, currency or completeness of the information. Neither the department nor the State of Western Australia nor any employee or agent of the department shall be responsible or liable for any loss, damage or injury arising from the use of or reliance on any information, data or advice (including incomplete, out of date, incorrect, inaccurate or misleading information, data or advice) expressed or implied in, or coming from, this publication or incorporated into it by reference, by any person whosoever.



Published 2022 by the Geological Survey of Western Australia

This Record is published in digital format (PDF) and is available online at <www.dmirs.wa.gov.au/GSWApublications>.

© **State of Western Australia (Department of Mines, Industry Regulation and Safety) 2022**

With the exception of the Western Australian Coat of Arms and other logos, and where otherwise noted, these data are provided under a Creative Commons Attribution 4.0 International Licence. (<https://creativecommons.org/licenses/by/4.0/legalcode>)

Further details of geoscience products are available from:

First floor counter
Department of Mines, Industry Regulation and Safety
100 Plain Street
EAST PERTH WESTERN AUSTRALIA 6004
Telephone: +61 8 9222 3459 Email: publications@dmirs.wa.gov.au
www.dmirs.wa.gov.au/GSWApublications

Cover image: Journey to the centre of the Kimberley (© 2010 PL Schubert)

Contents

| | |
|--|----|
| Abstract | 1 |
| Introduction | 1 |
| Olympus Vanta M-Series pXRF | 2 |
| Limitations of portable XRF analysis | 3 |
| Accuracy and precision | 4 |
| Calibration by certified reference materials | 4 |
| Count times | 18 |
| Grain size | 18 |
| Sampling intervals | 19 |
| Comparison with other methods | 19 |
| Minalyzer CS – XRF core scanner | 19 |
| Partial least squares spectral modeling | 30 |
| Case studies | 30 |
| Fraser Zone Exploration Incentive Scheme drillhole 20NMDD025 | 30 |
| Southern Carnarvon Basin GSWA Barrabiddy 1 well | 33 |
| Core library services | 38 |
| Access to downhole portable XRF data | 38 |
| Requests for portable XRF analysis | 38 |
| Requests for benchtop XRD analysis | 38 |
| Conclusions | 38 |
| References | 39 |

Figures

| | |
|---|----|
| 1. Olympus Vanta M-Series pXRF analyser with soil foot attachment | 2 |
| 2. Comparison of average crustal abundances of elements against corresponding limits of detection and quantification | 4 |
| 3. Calibration plot of measured Ca concentration (ppm) by the Vanta M-Series pXRF | 8 |
| 4. Comparative plots of calculated calibration for R ² values and linear slopes for significant elements | 9 |
| 5. Greenbushes Li deposit pegmatite specimen GSWA 201965 | 18 |
| 6. Coarse-grained (5–7 mm) intermediate igneous intrusion from 215 m in drillcore 18JBDD002 (M0002838) | 18 |
| 7. Comparative plots of randomly sampled measurements by the Vanta M-Series pXRF | 22 |
| 8. Regional geology and location of the 18JBDD002 drillhole | 23 |
| 9. Comparative downhole plots of ICP-MS and Vanta M-Series pXRF assays (ppm) of drillcore 18JBDD002 | 24 |
| 10. Comparative correlation plots of measurements (ppm) of 18JBDD002 half-core samples by the Vanta M-Series pXRF and Minalyzer XRF | 28 |
| 11. Comparative downhole plots of ICP-MS and Minalyzer XRF assays (ppm) of drillcore 18JBDD002 | 29 |
| 12. Comparative downhole plots of ICP-MS against PLS-predicted Mg and Zr, and Minalyzer measurements for Mg and Zr | 31 |
| 13. Regional geology and location of drillhole 20NMDD025 | 32 |
| 14. Simplified system-automated HyLogger downhole mineral logs for drillhole 20NMDD025 | 32 |
| 15. Comparative downhole plots of ICP-AES and Vanta M-Series pXRF assays (ppm) of drillcore 20NMDD025 | 34 |
| 16. Comparative plots of downhole system-automated phosphate mineral abundance measurements from HyLogger thermal infrared scan data and Vanta M-Series pXRF-measured P concentration | 35 |
| 17. Regional geology and location of the GSWA Barrabiddy 1 | 36 |
| 18. Simplified system-automated downhole mineral logs for GSWA Barrabiddy 1 | 36 |
| 19. Comparative downhole plots of ICP-AES/ICP-MS and Vanta M-Series pXRF assays (ppm) of drillcore GSWA Barrabiddy 1 | 37 |

Tables

| | |
|---|----|
| 1. Default element suite for the Olympus Vanta M-Series pXRF in GeoChem 3-beam mode | 2 |
| 2. Limits of detection and average crustal abundance for the default element suite for the Olympus Vanta M-Series pXRF in GeoChem 3-beam mode..... | 3 |
| 3. Certified composition of pressed powder pellet reference NCS DC 73308 | 5 |
| 4. Reference material compositions used for assessing the performance and calibration of the Olympus Vanta M-Series pXRF | 6 |
| 5. Linear correlation values for measurements of reference materials by the Olympus Vanta M-Series | 7 |
| 6. Statistics for the Olympus Vanta M-Series analyses of pressed powder reference material KG-1 | 10 |
| 7. Statistics for the Olympus Vanta M-Series analyses of pressed powder reference material BB-1 | 11 |
| 8. Statistics for the Olympus Vanta M-Series analyses of pressed powder reference material MW-1 | 12 |
| 9. Statistics for the Olympus Vanta M-Series analyses of pressed powder reference material NEWN305..... | 13 |
| 10. Statistics for the Olympus Vanta M-Series analyses of pressed powder reference material BIR-1a | 14 |
| 11. Statistics for the Olympus Vanta M-Series analyses of pressed powder reference material W-2..... | 15 |
| 12. Statistics for the Olympus Vanta M-Series analyses of pressed powder reference material TILL-1 | 16 |
| 13. Statistics for the Olympus Vanta M-Series analyses of pressed powder reference material STSD-4..... | 17 |
| 14. Statistics for the Olympus Vanta M-Series analyses in standard GeoChem 3-beam mode for coarse-grained rock sample GSWA 2019656 | 20 |
| 15. Statistics for the Olympus Vanta M-Series analyses in standard GeoChem 3-beam mode for a coarse-grained rock sample from drillcore 18JBDD002..... | 21 |
| 16. Measured concentrations of half-core samples by PANalytical MagiX Fast XRF..... | 25 |
| 17. Measured concentrations of half-core samples by the Minalyzer CS XRF core scanner | 26 |
| 18. Measured concentrations of half-core samples by Olympus Vanta M-Series pXRF | 27 |

Portable XRF analysis in the Joe Lord and Perth Core Libraries — methodology and case studies

by

MJ Wawryk and EA Hancock

Abstract

The Olympus Vanta M-Series (Rh-anode) portable X-ray fluorescence (pXRF) analyser enables the capture of downhole geochemical assays complementary to hyperspectral core logging, and has additional applications, including validation of spectral mineralogy. The instrument is currently capable of measuring 39 geologically important elements between Mg and U to parts-per-million (ppm) levels, with suitably accurate and precise results attained using the adopted total count time of 40 seconds (i.e. 20, 10, and 10 seconds per filter). Collection and provision of geochemical assay data using the Vanta pXRF and mineralogical analysis using the BTX-II pXRD, from materials stored in public collections has been incorporated into the GSWA HyLogger workflow, and is now available as a complimentary service at the GSWA Core Library facilities.

Measurement of in-house reference materials confirms excellent correlation with certified values using default factory calibration, with improved precision and accuracy observed in comparison with older-generation Thermo Fisher Niton XL3t GOLDD+ pXRF instruments, while reducing collection times by one-third. A comparison of analyses of samples with varied grain sizes shows that single measurements on coarse-grained rock (e.g. >5 mm) are sufficiently statistically robust to be considered representative for the purposes of observing geochemical trends, although very coarse-grained material (e.g. >10 mm pegmatites) requires multiple measurements to be sufficiently characterized.

A consistent, non-biased collection of single-shot measurements by the GSWA Vanta pXRF along drillcore at a density of one measurement per tray (i.e. every 3–5 m), accurately reproduced the downhole geochemical trends provided by time- and cost-intensive (but more sensitive) laboratory assay techniques, including inductively coupled plasma mass spectrometry and inductively coupled plasma atomic emission spectroscopy, both in major and trace elements. Extrapolation of higher-resolution downhole assays using partial least squares regression modeling of downhole HyLogger spectral data also accurately replicated broad trends as well as defined anomalous geochemical features, as confirmed by the high-resolution XRF analysis of core by Minalyzer CS core logging.

KEYWORDS: core logging, drillcore, geochemistry, HyLogger, hyperspectral, petrology, trace element, X-ray fluorescence

Introduction

Geochemical analysis is one of many fundamental tools for measurement and interpretation of rocks, soils, and other geological materials. Geochemical studies provide information on various geological aspects, including classifying lithology, determining petrogenesis and provenance, constraining alteration and metamorphic history, and quantifying mineralogy and mineralization. Among the numerous geochemical analytical techniques available to geoscientists, X-ray fluorescence (XRF) spectroscopy is one of the most commonly utilized due to its speed, sensitivity, and minimal sample preparation (Morris, 2009).

XRF analysis uses a collimated beam of primary X-rays to excite electrons in the atoms of an analysed material, which release secondary X-rays upon returning to their ground state, in a phenomenon referred to as XRF (Klein and Dutrow, 2007; Morris, 2009). The energies of the secondary X-rays are characteristic of their corresponding element, enabling detection and quantification of various elements in the sample (Klein and Dutrow, 2007; Morris, 2009). Although initially confined to laboratory-based instruments, the development of field-portable XRF (pXRF) instruments in recent decades

now enable geoscientists to facilitate real-time in situ geochemical assaying of samples (Lemière and Harmon, 2021; Piorek, 2021).

Continued development and refinements in pXRF technologies and workflows have resulted in increasingly sensitive and accurate measurements of wider ranges of geologically important elements, prompting their uptake and routine use in industry and academia (Morris, 2009; Lemière and Harmon, 2021). Recent advances include accurate measurement of lighter elements (e.g. Mg, Al, Si) without need of a vacuum or helium flush, improvements in analytical algorithms, and continued reduction in collection and processing times (Lemière and Harmon, 2021). Morris (2009) provides an introductory guide to the use, advantages, and complications of pXRF analysis, which has been used by GSWA for over a decade.

In recent years, there has been an increasing desire to regularly incorporate and correlate geochemistry with downhole spectral data routinely collected from drillcore with the GSWA HyLogger 3-2 system to improve lithological characterization, detect geochemical trends or anomalies, and assist in spectral unmixing and mineral validation for unusual, ambiguous or non-unique spectral responses.

HyLogger-3 utilizes infrared reflectance (IR) spectroscopy to collect direct physicochemical measurements of geological samples with the size and position of observed reflection or absorption features and provides mineralogical information, including mineral abundance, crystallinity, grain size, and relative chemistry of solid solutions (Hancock et al., 2013).

For the purposes of collecting geochemical trend data, pXRF analysis is considered a suitable complementary technique to the rapid, non-destructive hyperspectral data collected by the GSWA HyLogger 3-2, because absolute accuracy and very low detection limits for trace elements are not critically important in this case. The rapid data-capturing ability and simplicity of pXRF instruments are ideal for incorporation in current HyLogger workflows, and enable the collection of spatially co-located IR and XRF spectral measurements. Although geochemical drillcore assays are often collected by mineral companies, these assays can be biased or limited in scope towards areas and elements of interest, and geochemical assays typically do not exist for historical drillholes or petroleum core.

Using pXRF analysis alongside HyLogger-3 core scanning enables real-time collection of downhole geochemical assays for a wide range of important elements, which can be guided by spectral interpretation and in turn, direct further sampling and analysis. The aim of this record is to detail the advantages of and provide an example workflow for collecting consistent and non-biased geochemical assays using pXRF analysis.

Olympus Vanta M-Series pXRF

In 2020, GSWA purchased a new field-portable XRF analyser, an Olympus Vanta M-Series pXRF (Fig. 1). This next-generation instrument supplements the existing pXRF analysers used by GSWA (Morris, 2009) and was acquired primarily to provide complementary geochemistry data for downhole spectral mineralogy generated by the GSWA HyLogger-3 system. This energy-dispersive XRF analyser can detect and measure concentrations of 39 geologically important elements between Mg and U to parts-per-million (ppm) levels in the default factory configuration, utilizing the 3-beam GeoChem mode (Olympus, 2018).

Beam 1 (40 kV) is used to detect elements between Ti and U, beam 2 (10 kV) for elements between Mg and Mn, and beam 3 (50 kV) for elements between Ag to Nd, with some overlap of elements (Table 1). Many elements are currently not measured in the default factory configuration to maximize instrumental accuracy and geological utility, although they can be subsequently incorporated by Olympus upon request.



Figure 1. Olympus Vanta M-Series portable XRF analyser with soil foot attachment

Reasons for exclusion of an element include perceived lack of significant geological value (e.g. Cs), elemental interference (e.g. Au with Pt), insufficient energy of the primary X-ray beam (e.g. HREE), lack of access to suitable standards (e.g. Os), and interference with the chosen X-ray anode (e.g. Cl with Rh-anode) (Olympus, 2020; Bailey, 2021, written comm., 26 March).

The general configuration of the Olympus Vanta is analogous to other pXRF analysers (cf. Morris, 2009), consisting primarily of an X-ray source and various filters, detector, aiming camera, processing hardware, and a Li-ion battery power source. The instrument can be operated using its integrated touchscreen and buttons or via a remote control using the Vanta software application on a computer or android-based device. Users can connect to the device via a USB cable, Bluetooth or Wi-Fi. The collected data can be exported wirelessly to the cloud or networked location, physically via the Vanta software application or directly to storage devices using the available USB ports (Olympus, 2021).

The M-series model selected by GSWA utilizes a 4-watt X-ray tube with an Rh-anode (8-50 keV) excitation source, replaceable 6-µm prolene measurement windows, and a large area silicon drift detector with ~140 eV resolution (Olympus, 2016, 2019). This model also incorporates a 0.9-µm graphene window that reduces the attenuation of X-rays compared to traditional thicker beryllium windows used in older pXRF analysers. This increases the sensitivity of the detector to and reduces detection limits of geologically important light elements, including Mg, Al,

Table 1. Default element suite for Olympus Vanta M-Series pXRF in GeoChem 3-beam mode

| Beam | Energy | Detectable elements |
|------|--------|--|
| 1 | 40 kV | Ti, V, Cr, Mn, Fe, Co, Ni, Cu, Zn, As, Se, Rb, Sr, Y, Zr, Nb, Mo, Ag, Cd, Sn, Sb, Ba, W, Hg, Pb, Bi, Th, U, LE |
| 2 | 10 kV | Mg, Al, Si, P, S, K, Ca, Ti, Mn |
| 3 | 50 kV | Ag, Cd, Sn, Sb, Ba, La, Ce, Pr, Nd, LE |

Notes: LE, Light elements, inferred combined abundance of elements H to Na by measurement of the background Compton peak (Brouwer, 2010; Olympus, 2020)

and Si (Olympus, 2016, 2020). A collimated 8-mm diameter area comparable to the measurement area of the GSWA HyLogger-3 instrument (Hancock and Huntington, 2010) is analysed, assisting with direct comparison to IR spectral measurements.

The Olympus Vanta series of pXRF analysers utilize Olympus' new Axon™ technology, which incorporates proprietary ultra-low-noise electronics and enhanced signal processing (Olympus, 2016). The resulting improvement in X-ray count rates reduces testing times and improves detection limits and precision, requiring one-half to one-third of the collection time of the preceding Thermo Fisher Niton XL3t GOLDD+ pXRF analyser in practice. The Olympus Vanta also performs near-instantaneous energy checks and drift corrections before every measurement, resulting in highly stable and repeatable results, and limits the instrumental drift that affects all pXRF analysers (Rousseau, 2002; Olympus, 2016).

Limitations of portable XRF analysis

Although technological advances have improved the accuracy and utility of pXRF instruments, several fundamental limitations remain for this technique. Minimum detection levels for most elements are limited to ppm, and elements lighter than Mg are generally considered undetectable due to strong attenuation of their weak XRF (Lemière and Harmon, 2021; Piorek, 2021). Although several elements, including Au, Ag, Hg, and Cd, are capable of detection by XRF analysis, their low natural concentration in many geological materials means pXRF instruments are generally unsuitable for reliable detection and measurement (Morris, 2009; Lemière and Harmon, 2021).

The limits of detection ([LOD], three times the uncertainty [3σ]) and limits of quantification ([LOQ]; 10 times the uncertainty [10σ]) inform the user, whether a measurement is reliable for detecting and quantifying elements, respectively, and reduces with increasing collection time (Olympus, 2020). The user should treat measurements below these values with caution and these may need to be excluded from the statistics. The absolute LOD and LOQ of default elements using Vanta in the GeoChem mode, as measured by Olympus using interference-free silica blanks and 120-second beam measurement times, are listed in Table 2 (Rudnick and Gao, 2014; Olympus, 2018). By default, calculated element concentrations of the analytes are presented by the Olympus Vanta together with their 1σ uncertainty values.

A comparison against average crustal elemental abundances (Fig. 2) indicates that the Olympus Vanta instrument is sufficiently sensitive to detect and quantify Mg–Zn + Rb–Nb + Ba + Pb in typical crustal rocks, which constitute a majority of geologically important bulk and trace elements. The remaining elements require further concentrating by geological processes to be detectable in measured samples, such as mineralization or supergene enrichment.

The point measurements collected by pXRF instruments are generally less accurate and precise than those acquired by laboratory-based XRF instruments due to the trade-off of using

Table 2. Limits of detection (LOD) and average crustal abundance for default element suite for Olympus Vanta M-Series pXRF in GeoChem 3-beam mode

| Element | Average crustal abundance (ppm)* | Vanta LOD (ppm) ^a |
|---------|----------------------------------|------------------------------|
| Mg | 28350 | 1100 |
| Al | 84150 | 95 |
| Si | 283300 | 160 |
| P | 436 | 10 |
| S | 404 | 13 |
| K | 14950 | 16 |
| Ca | 45750 | 17 |
| Ti | 4200 | 25 |
| V | 138 | 4 |
| Cr | 135 | 8 |
| Mn | 770 | 5 |
| Fe | 52080 | 12 |
| Co | 26.6 | 5 |
| Ni | 59 | 4 |
| Cu | 27 | 2 |
| Zn | 72 | 1 |
| As | 2.5 | 1 |
| Se | 0.13 | 1 |
| Rb | 49 | 1 |
| Sr | 320 | 1 |
| Y | 21.9 | 1 |
| Zr | 132 | 1 |
| Nb | 8 | 2 |
| Mo | 0.8 | 1 |
| Ag | 0.056 | 2 |
| Cd | 0.08 | 2 |
| Sn | 1.7 | 2 |
| Sb | 0.2 | 2 |
| Ba | 456 | 10 |
| La | 20 | 40 |
| Ce | 43 | 40 |
| Pr | 4.9 | 30 |
| Nd | 20 | 60 |
| W | 1 | 1 |
| Hg | 0.03 | 1 |
| Pb | 11 | 2 |
| Bi | 0.18 | 1 |
| Th | 5.6 | 2 |
| U | 1.3 | 1 |

Notes: *Converted from Rudnick and Gao (2014); ^aOlympus (2018); LOD, limits of detection

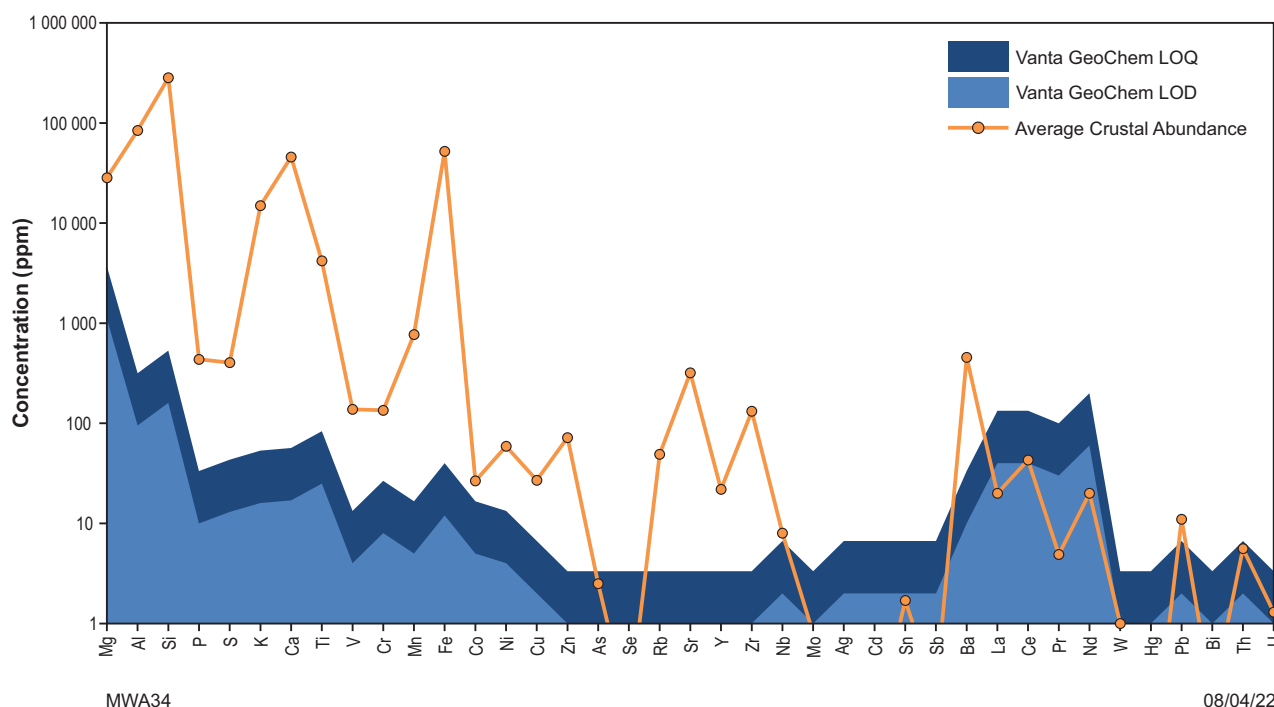


Figure 2. Comparison of average crustal abundances of elements against corresponding limits of detection (LOD) and limits of quantification (LOQ) for Olympus Vanta M-Series pXRF for the default Vanta 3-beam GeoChem elemental suite. Modified from Rudnick and Gao (2014) and Olympus (2018)

the more rapid simultaneous multi-element measurements of the energy-dispersive XRF method, compared to the slower but higher-resolution wavelength-dispersive XRF method (Brouwer, 2010). The consequent overlap of XRF peaks beyond resolution limits in energy-dispersing pXRF analysers (e.g. Co K β -peak at 6.93 keV and Fe K α -peak at 7.06 keV) can cause over- or underestimation of the corresponding elements (Olympus, 2020).

Causes of peak overlap include elemental interference (coincidence of fundamental elemental peaks), sum peaks (simultaneous measurement of two X-ray photons resulting in the summation of both peak energies), peak broadening (observed with increasing concentration of an element), and escape peaks (caused by excitation of silicon in the detector resulting in peaks with an energy 1.74 keV below the causative elemental peak energy) (Brouwer, 2010; Gallhofer and Lottermoser, 2018). These effects are matrix-dependent and correlate with the causative elemental concentrations (e.g. elements with high concentrations will cause larger sum peaks).

The analytical algorithm of the Olympus Vanta's GeoChem mode, which uses the fundamental parameters method to model the interaction of every element with each other (Olympus, 2020), accounts for the effects of peak overlap. Fundamental parameters can account for various effects, including peak overlap, sum and escape peaks, X-ray absorption, and secondary fluorescence (Rousseau, 2013; Olympus, 2020). Although this enables more accurate quantification of elements, it requires significantly more computational power than simpler methods (e.g. Compton scattering method used in the Thermo Fisher Niton's soil mode) (Kawai et al., 2019; Olympus, 2020).

Variations in sample composition and condition (e.g. grain size, heterogeneity, water content, matrix effects) can impact the results; therefore, repeated measurements of

and calibration against suitable certified reference materials (CRM) or project-based standard reference materials (SRM) are necessary for accurate measurements (Gallhofer and Lottermoser, 2018; Lemi re and Harmon, 2021). However, the use of fundamental parameters in the Vanta GeoChem mode ensures that quantification of uncalibrated materials with factory calibration remain relatively accurate and can be improved with user calibrations against known standards (Brouwer, 2010; Olympus, 2020).

Accuracy and precision

Calibration by certified reference materials

The accuracy (closeness of a measurement to its true value) and precision (consistent repeatability of a measurement result) of pXRF analysis relies on sufficient calibration of the instrument, using suitable reference materials with known values (e.g. CRMs). These reference materials need to cover a broad range of elemental concentrations and matrix types comparable to the intended analysis materials, to ensure accurate results (Morris, 2009; Olympus, 2020; Piorek, 2021). Olympus performs machine-specific calibration on Vanta pXRFs during manufacture (factory calibration), although further project specific calibrations (user factors) can be determined and applied by the user. Routine drift monitoring and calibration on the GSWA-owned instrument is performed using pressed powder reference NCS DC 73308 (Table 3).

To test the accuracy and precision of factory calibrations, measurements were taken on a series of pressed powder pellet CRMs and GSWA SRMs representing a range of typical crustal materials (Table 4). Factory-calibrated analytical

Table 3. Certified composition of pressed powder pellet reference NCS DC 73308 used for drift monitoring and calibration of the Olympus Vanta M-Series pXRF

| Element | Certified concentration (ppm) ^a |
|---------|--|
| Mg | 724 |
| Al | 15031 |
| Si | 415507 |
| P | 271 |
| S | 90 |
| K | 1038 |
| Ca | 7000 |
| Ti | 1271 |
| V | 107 |
| Cr | 136 |
| Mn | 1007 |
| Fe | 26998 |
| Co | 15.3 |
| Ni | 30.2 |
| Cu | 22.6 |
| Zn | 46 |
| As | 8.4 |
| Se | 0.28 |
| Rb | 9.2 |
| Sr | 25.3 |
| Y | 13.8 |
| Zr | 70 |
| Nb | 6.8 |
| Mo | 1.2 |
| Ag | 0.27 |
| Cd | 1.12 |
| Sn | 1.4 |
| Sb | 6.3 |
| Ba | 430 |
| La | 13 |
| Ce | 38 |
| Pr | 3.2 |
| Nd | 11.8 |
| W | 1.63 |
| Hg | 280 |
| Pb | 27 |
| Bi | 0.38 |
| Th | 5 |
| U | 2.1 |

Notes: ^aModified from Fluxana (Fluxana, 2015); NCS, NCS Testing Technology Co., Ltd

results from the pressed powder pellets for detectable elements with sufficient samples were plotted against certified element concentrations, and lines of best fit calculated for respective beam times (regression parameters in Table 5). Measurements of standards with concentrations below detection limits, concentration orders of magnitudes larger than the remaining standards, and significant outliers were excluded from the calculations to ensure a more representative sample. An example calibration plot for Ca shows excellent correlation with the certified concentrations (Fig. 3). Calibration plots for most elements show high degrees of linear correlation with R^2 values >0.95 , with exception for the results for P, Ti, and Zn (Fig. 4a). The calibration factors required to correct Vanta measurements (Fig. 4b) are generally small and typically range between 0.8 and 1.2.

Analytical results for the eight reference materials (Tables 6–13) demonstrate that Mg–Si + Ca–Fe + Ni–Zn + Rb–Zr + Ba + Pb have good correlations with certified values. The measurements of these elements generally show high precision with relative standard deviations ([RSD]; i.e. $100 \times (\text{standard deviation}/\text{mean})$) of <10 and high accuracy with half relative deviations ([HRD]; i.e. $|100 \times (\text{certified value} - \text{mean}) / (\text{certified value} + \text{mean})|$) of $<10\%$. Results for Si, Al, Ca, Mn, Fe, Sr, and Zr in particular, show very good precision and accuracy with RSD and HRD, frequently $<2\%$. These results are typical of pXRF instrumental performance (Lemière and Harmon, 2021) and superior to the results obtained with the Niton XL3t GOLDD+ (Morris, 2009).

Analytical results for Mg, P, S, and K show good precision and accuracy when above the LOQ, with RSD and HRD values typically between 5% and 10%, although RSD is observed to significantly decrease with increasing concentration. Lighter elements are known to have weaker fluorescence, increased Compton scattering of primary X-rays, and increased overlaps due to the density of fluorescence peaks at their lower fluorescence energies. This complicates detection and deconvolution with pXRF analysers, reducing their precision and accuracy of analytical results at lower concentrations (Brouwer, 2010). Nickel, Cu, Zn, and As are observed to have good precision and accuracy when above the LOQ, although abundances of these elements in the measured references are commonly below the LOD, preventing consistent detection. Similarly Se, Nb, and most heavier elements are inconsistently detected.

Cobalt is consistently observed to have poor precision and accuracy with RSD% and HRD values typically $>15\%$, likely caused by concentrations in the measured references being close to the LOQ, and peak overlap with the more abundant Fe (Olympus, 2020). Analytical results for the CRM NEWN305 do not show good correlation with the certified values, with HRD values $>15\%$, although most elements show good precision with RSD $<10\%$. As suggested by Morris (2009), this could be due to matrix effects due to the higher proportion of Fe-oxides and lower proportion of Si in this reference sample when compared to typical unaltered silicate rocks. Therefore, factory calibration of the Olympus Vanta may not be sufficient for accurate analysis of some elements in non-silicate and relatively silica-poor rocks, including carbonates, evaporites, and some regolith. As per good pXRF practices, the user should improve the calibration of the instrument for analysis of such materials (Brouwer, 2010; Olympus, 2020).

Table 4. Reference material compositions used for assessing the performance and calibration of the Olympus Vanta M-Series pXRF

| | GSWA | | | | USGS | | CCRMP | |
|-----------------|---------------------|---------------|-------------------------|----------------------------|---------------------------|------------------------|---------------------------|---------------------------|
| <i>Standard</i> | <i>KG-1*</i> | <i>BB-1*</i> | <i>MW-1^v</i> | <i>NEWN305^v</i> | <i>BIR-1a^A</i> | <i>W-2^A</i> | <i>TILL-1^A</i> | <i>STSD-4^A</i> |
| <i>Source</i> | <i>Monzogranite</i> | <i>Basalt</i> | <i>Komatiite</i> | <i>Laterite</i> | <i>Basalt</i> | <i>Dolerite</i> | <i>Till</i> | <i>Stream Sediment</i> |
| <i>Element</i> | <i>(ppm)</i> | <i>(ppm)</i> | <i>(ppm)</i> | <i>(ppm)</i> | <i>(ppm)</i> | <i>(ppm)</i> | <i>(ppm)</i> | <i>(ppm)</i> |
| Mg | 2895 | 28463 | 185310 | 302 | 58494 | 38413 | 12965 | 12664 |
| Al | 79121 | 81133 | 23445 | 133051 | 82032 | 81768 | 72506 | 64038 |
| Si | 333614 | 242207 | 190857 | 92273 | 224186 | 246249 | 284673 | 275324 |
| P | 349 | 1091 | 960 | 175 | 92 | 611 | 960 | 873 |
| S | 75 | 399 | - | 899 | - | 79 | - | 900 |
| K | 28806 | 3819 | 664 | 249 | 249 | 5197 | 18429 | 13282 |
| Ca | 15437 | 62250 | 29588 | 214 | 95054 | 77616 | 19440 | 28588 |
| Ti | 1439 | 12108 | 1319 | 13367 | 5754 | 6354 | 5874 | 1199 |
| V | 14.6 | 245 | 89 | 472 | 310 | 260 | 99 | 106 |
| Cr | 170 | 150 | 1920 | 3225 | 370 | 92 | 65 | 93 |
| Mn | 310 | 1239 | 1084 | 155 | 1355 | 1293 | 1394 | 1549 |
| Fe | 14549 | 85472 | 66937 | 268868 | 79038 | 75750 | 47702 | 39869 |
| Co | 3 | 37 | 107 | 28 | 52 | 43 | 18 | 13 |
| Ni | 8 | 41 | 2214 | 314 | 170 | 70 | 24 | 30 |
| Cu | 6 | 82 | 41 | 1036 | 125 | 110 | 47 | 65 |
| Zn | 41 | 116 | 59 | 111 | 70 | 80 | 98 | 107 |
| As | 1 | 5.2 | 2.3 | 52 | 0.44 | 1.2 | 18 | 15 |
| Se | - | - | - | 1.3 | - | - | - | - |
| Rb | 96 | 12.4 | 2.4 | 6 | - | 21 | 44 | 39 |
| Sr | 515 | 245 | 11 | 4 | 110 | 190 | 291 | 350 |
| Y | 4.5 | 39.8 | 6 | 5 | 16 | 23 | 38 | 24 |
| Zr | 190 | 153 | 11 | 146 | 18 | 100 | 502 | 190 |
| Nb | 9.5 | 7.6 | 0.4 | 6 | 0.6 | 7.9 | 10 | 9 |
| Mo | 2 | 1.8 | - | 4 | - | - | 2 | 5 |
| Ag | 0.01 | - | - | - | - | - | - | - |
| Cd | - | - | - | - | - | - | - | - |
| Sn | 1.8 | 1.8 | - | 2 | - | - | - | 2 |
| Sb | 3.6 | 0.3 | 2.5 | 2.6 | 0.58 | 0.79 | - | 7.3 |
| Ba | 1373 | 152 | 24 | 22 | 7 | 170 | 702 | 2000 |
| La | 44 | 10.95 | 2.1 | 2 | 0.63 | 10 | 28 | 24 |
| Ce | 71 | 26.8 | 2 | 8 | 1.9 | 23 | 71 | 44 |
| Pr | 6.6 | 3.63 | 0.3 | - | - | - | - | - |
| Nd | 22.4 | 18.75 | 1.5 | - | - | 13 | 26 | 21 |
| W | - | - | 47 | - | - | - | - | - |
| Hg | - | - | - | 35 | - | - | - | - |
| Pb | 40 | 4.4 | - | 16 | 3 | 9.3 | 22 | 16 |
| Bi | 2 | - | 0.2 | 0.6 | - | - | - | - |
| Th | 17.4 | 1.8 | - | 14 | - | 2.4 | 5.6 | 4.3 |
| U | 4.2 | 0.3 | - | 3 | - | - | 2.2 | 3 |

Notes: USGS, United States Geological Survey; CCRMP, Canadian Certified Reference Materials Project; *Modified from Morris (2007); ^vGSWA unpublished data, Morris (2009); ^AModified from Fluxana (Fluxana, 2015)

Table 5. Linear correlation values for measurements of reference materials by the Olympus Vanta M-Series in Geochem 3-beam mode

| Element | Reference | | 10 seconds per beam | | | 20 seconds per beam | | | 30 seconds per beam | | |
|---------|---------------|---------------|---------------------|-----------|----------------|---------------------|-----------|----------------|---------------------|-----------|----------------|
| | Min. (ppm) | Max. (ppm) | Slope | Intercept | R ² | Slope | Intercept | R ² | Slope | Intercept | R ² |
| Mg | 12965 | 185310 | 0.865 | 10420 | 0.980 | 0.869 | 10921 | 0.980 | 0.884 | 9918 | 0.980 |
| Al | 23445 | 133305 | 0.811 | 11146 | 0.966 | 0.787 | 12151 | 0.963 | 0.809 | 10797 | 0.968 |
| Si | 92273 | 333614 | 1.169 | -28566 | 0.993 | 1.159 | -29631 | 0.994 | 1.153 | -25519 | 0.991 |
| P | 349 | 960 | 0.595 | 339 | 0.721 | 0.596 | 329 | 0.687 | 0.608 | 344 | 0.700 |
| K | 1091 | 28806 | 1.061 | 45.21 | 0.982 | 1.060 | 15.77 | 0.982 | 1.062 | 41.52 | 0.981 |
| Ca | 15437 | 95054 | 1.019 | 1686 | 0.996 | 1.027 | 1603 | 0.996 | 1.022 | 1666 | 0.996 |
| Ti | 1199 | 13367 | 1.222 | -984 | 0.773 | 1.193 | -820 | 0.765 | 1.226 | -916 | 0.777 |
| Mn | 155 | 1549 | 1.076 | -4.39 | 0.989 | 1.088 | -17.92 | 0.985 | 1.072 | -3.65 | 0.990 |
| Fe | 14549 | 268868 | 1.262 | -12550 | 0.995 | 1.268 | -12920 | 0.994 | 1.262 | -12679 | 0.995 |
| Ni | 24 | 170 | 1.055 | -17.82 | 0.990 | 0.981 | -10.73 | 0.996 | 0.970 | -10.76 | 0.996 |
| Cu | 47 | 125 | 0.850 | 8.02 | 0.959 | 0.915 | 1.02 | 0.963 | 0.942 | 0.43 | 0.969 |
| Zn | 41 | 116 | 0.920 | 0.01 | 0.695 | 0.910 | 2.25 | 0.779 | 0.977 | -1.27 | 0.806 |
| Rb | 2 | 96 | 1.008 | 0.95 | 0.987 | 0.997 | 1.63 | 0.991 | 0.999 | 1.73 | 0.992 |
| Sr | 11 | 515 | 0.966 | 2.38 | 0.999 | 0.954 | 6.16 | 0.999 | 0.961 | 5.26 | 0.999 |
| Y | 16 | 40 | 1.045 | -1.31 | 0.980 | 1.014 | -0.40 | 0.986 | 1.020 | 0.46 | 0.985 |
| Zr | 11 | 502 | 1.092 | -4.60 | 0.992 | 1.092 | -8.50 | 0.987 | 1.086 | -2.26 | 0.994 |
| Ba | 152 | 2000 | 0.913 | -130 | 0.992 | 0.945 | -61.04 | 0.997 | 0.913 | -116 | 0.995 |
| Pb | 9 | 40 | 1.246 | -5.30 | 0.982 | 1.185 | -3.89 | 0.963 | 1.171 | -3.73 | 0.987 |

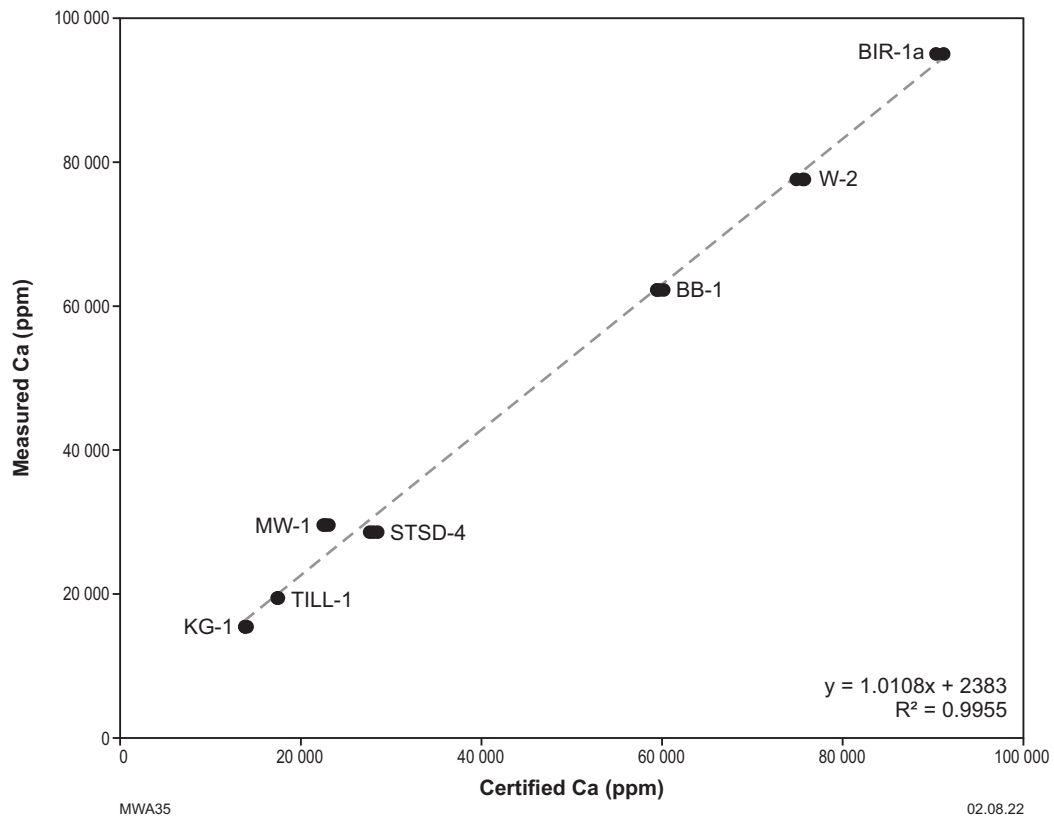


Figure 3. Calibration plot of measured Ca concentration (ppm) by the Vanta M-Series pXRF in default factory-calibrated 3-beam GeoChem mode against recommended values of pressed powder reference standards BB-1, BIR-1a, KG-1, MW-1, STSD-4, TILL-1, and W-2. Line of best fit and statistics are computer generated. The R^2 value close to 1 indicates very high correlations between measured and recommended concentrations and the calculated slope suggests an average overestimation of Ca by approximately 1% across this range of concentrations

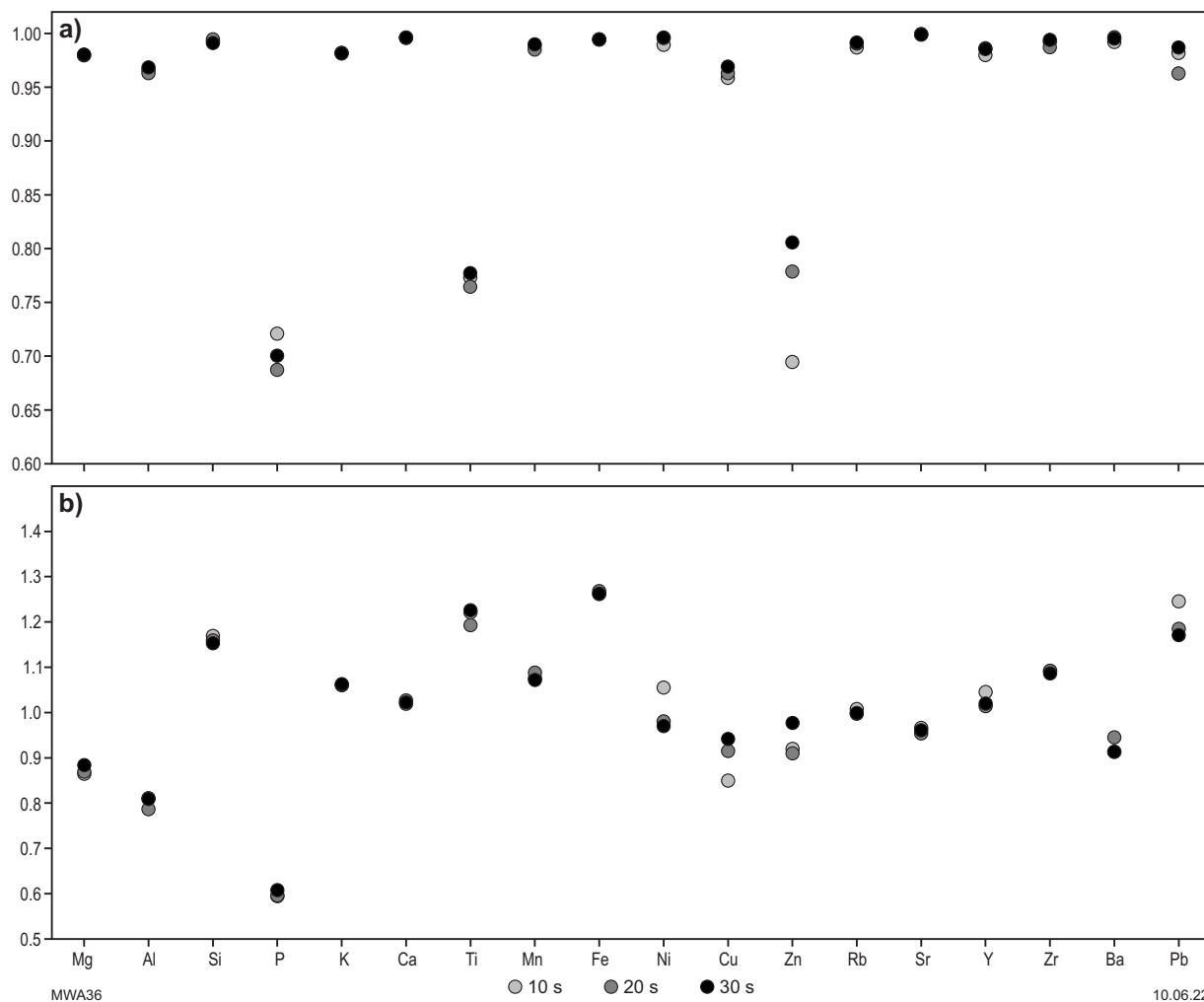


Figure 4. Comparative plots of calculated calibration: a) R^2 values; b) linear slopes for significant elements measured by the Vanta pXRF in 3-beam GeoChem mode, showing the effect of setting collection times per beam of 10, 20, and 30 seconds. R^2 values close to 1 indicate high correlations between measured and reference concentrations. Linear slopes >1 indicate an overestimation of concentrations, and vice versa. Detailed values are presented in Table 4

Table 6. Statistics for Olympus Vanta M-Series analyses of pressed powder reference material KG-1 in standard GeoChem 3-beam mode

| Element | Certified conc. (ppm) | Valid samples | Mean (ppm) | SD (ppm) | RSD (%) | Min. (ppm) | Max. (ppm) | Range (ppm) | HRD (%) |
|---------|-----------------------|---------------|------------|----------|---------|------------|------------|-------------|---------|
| Mg | 2895 | 0 | - | - | - | - | - | - | - |
| Al | 79121 | 9 | 74808 | 431 | 0.58 | 73911 | 75367 | 1456 | 2.80 |
| Si | 333614 | 9 | 315944 | 2122 | 0.67 | 312952 | 320192 | 7240 | 2.72 |
| P | 349.1 | 9 | 197 | 39.65 | 20.08 | 161 | 287 | 126 | 27.75 |
| S | 75 | 0 | - | - | - | - | - | - | - |
| K | 28806 | 9 | 28256 | 186 | 0.66 | 27913 | 28487 | 574 | 0.96 |
| Ca | 15437 | 9 | 13906 | 76.64 | 0.55 | 13809 | 14058 | 249 | 5.22 |
| Ti | 1439 | 9 | 1530 | 102 | 6.67 | 1400 | 1684 | 284 | 3.08 |
| V | 14.6 | 0 | - | - | - | - | - | - | - |
| Cr | 170 | 9 | 182 | 13.18 | 7.24 | 158 | 209 | 51 | 3.41 |
| Mn | 309.8 | 9 | 264 | 22.54 | 8.55 | 233 | 302 | 69 | 8.02 |
| Fe | 14549 | 9 | 14474 | 93.25 | 0.64 | 14353 | 14659 | 306 | 0.26 |
| Co | 3 | 3 | 27 | 31.65 | 117 | 0 | 87 | 87 | 80.00 |
| Ni | 8 | 0 | - | - | - | - | - | - | - |
| Cu | 6 | 0 | - | - | - | - | - | - | - |
| Zn | 41 | 9 | 46 | 2.49 | 5.42 | 43 | 50 | 7 | 5.75 |
| As | 1 | 0 | - | - | - | - | - | - | - |
| Se | 0.01 | 0 | - | - | - | - | - | - | - |
| Rb | 96 | 9 | 96 | 1.70 | 1.77 | 93 | 99 | 6 | 0.00 |
| Sr | 515 | 9 | 535 | 2.69 | 0.50 | 530 | 540 | 10 | 1.99 |
| Y | 4.5 | 6 | 4.17 | 1.34 | 32.25 | 2 | 6 | 4 | 3.85 |
| Zr | 190 | 9 | 191 | 3.53 | 1.84 | 185 | 197 | 12 | 0.35 |
| Nb | 9.5 | 9 | 5.00 | 1.56 | 31.27 | 3 | 8 | 5 | 31.03 |
| Mo | 2 | 9 | 6.56 | 1.95 | 29.75 | 4 | 10 | 6 | 53.25 |
| Ag | 0.01 | 1 | 9.00 | - | - | 9 | 9 | 0 | - |
| Cd | 0.01 | 0 | - | - | - | - | - | - | - |
| Sn | 1.8 | 3 | 17.33 | 1.89 | 10.88 | 16 | 20 | 4 | 81.18 |
| Sb | 3.6 | 0 | - | - | - | - | - | - | - |
| Ba | 1373 | 9 | 1677 | 74.02 | 4.41 | 1556 | 1765 | 209 | 9.97 |
| La | 44 | 6 | 114 | 23.29 | 20.46 | 68 | 140 | 72 | 44.24 |
| Ce | 71 | 7 | 135 | 26.06 | 19.24 | 92 | 167 | 75 | 31.21 |
| Pr | 6.6 | 0 | - | - | - | - | - | - | - |
| Nd | 22.4 | 0 | - | - | - | - | - | - | - |
| W | 0.01 | 0 | - | - | - | - | - | - | - |
| Hg | 0.01 | 0 | - | - | - | - | - | - | - |
| Pb | 40 | 9 | 35.89 | 1.52 | 4.245 | 34 | 39 | 5 | 5.42 |
| Bi | 2 | 0 | - | - | - | - | - | - | - |
| Th | 17.4 | 9 | 19.44 | 2.67 | 13.74 | 14 | 23 | 9 | 5.55 |
| U | 4.2 | 4 | 4.50 | 2.06 | 45.81 | 3 | 8 | 5 | 3.45 |

Notes: *Modified from Morris (2007); conc., concentration; SD, standard deviation; RSD, relative standard deviation ($100 \times (\text{SD}/\text{mean})$); HRD, half relative deviation ($100 \times (\text{certified value} - \text{mean}) / (\text{certified value} + \text{mean})$)

Table 7. Statistics for Olympus Vanta M-Series analyses of pressed powder reference material BB-1 in standard GeoChem 3-beam mode

| Element | Certified conc. (ppm) | Valid samples | Mean (ppm) | SD (ppm) | RSD (%) | Min. (ppm) | Max. (ppm) | Range (ppm) | HRD (%) |
|---------|-----------------------|---------------|------------|----------|---------|------------|------------|-------------|---------|
| Mg | 28463 | 9 | 22810 | 1404 | 6.16 | 20387 | 24972 | 4585 | 11.03 |
| Al | 81133 | 9 | 82493 | 763 | 0.93 | 81065 | 83270 | 2205 | 0.83 |
| Si | 242207 | 9 | 236162 | 1957 | 0.83 | 233059 | 239570 | 6511 | 1.26 |
| P | 1091 | 9 | 802 | 44.37 | 5.53 | 756 | 912 | 156 | 15.25 |
| S | 399 | 0 | - | - | - | - | - | - | - |
| K | 3819 | 9 | 2724 | 60.81 | 2.23 | 2600 | 2812 | 212 | 16.74 |
| Ca | 62250 | 9 | 59773 | 401 | 0.67 | 59154 | 60256 | 1102 | 2.03 |
| Ti | 12108 | 9 | 11860 | 140 | 1.18 | 11637 | 12082 | 445 | 1.03 |
| V | 245 | 9 | 303 | 52.66 | 17.39 | 241 | 412 | 171 | 10.55 |
| Cr | 150 | 9 | 112 | 10.43 | 9.30 | 97 | 126 | 29 | 14.41 |
| Mn | 1239 | 9 | 1142 | 18.64 | 1.63 | 1100 | 1160 | 60 | 4.10 |
| Fe | 85472 | 9 | 82870 | 484 | 0.58 | 82033 | 83695 | 1662 | 1.55 |
| Co | 37 | 8 | 178 | 28.16 | 15.83 | 136 | 229 | 93 | 65.56 |
| Ni | 41 | 9 | 58.00 | 4.42 | 7.62 | 53 | 65 | 12 | 17.17 |
| Cu | 82 | 9 | 81.11 | 5.22 | 6.43 | 75 | 92 | 17 | 0.55 |
| Zn | 116 | 9 | 121.10 | 2.60 | 2.15 | 117 | 126 | 9 | 2.16 |
| As | 5.2 | 7 | 5.14 | 0.35 | 6.80 | 5 | 6 | 1 | 0.55 |
| Se | 0.01 | 0 | - | - | - | - | - | - | - |
| Rb | 12.4 | 9 | 12.67 | 1.25 | 9.85 | 11 | 15 | 4 | 1.06 |
| Sr | 245 | 9 | 242 | 3.06 | 1.26 | 239 | 249 | 10 | 0.52 |
| Y | 39.8 | 9 | 40.11 | 1.60 | 3.98 | 37 | 42 | 5 | 0.39 |
| Zr | 153 | 9 | 153.40 | 1.77 | 1.15 | 151 | 156 | 5 | 0.15 |
| Nb | 7.6 | 5 | 4.40 | 0.49 | 11.13 | 4 | 5 | 1 | 26.67 |
| Mo | 1.8 | 9 | 8.89 | 2.81 | 31.57 | 4 | 15 | 11 | 66.32 |
| Ag | 0.01 | 0 | - | - | - | - | - | - | - |
| Cd | 0.01 | 3 | 21.33 | 5.79 | 27.15 | 15 | 29 | 14 | 99.91 |
| Sn | 1.8 | 6 | 28.17 | 6.77 | 24.03 | 22 | 39 | 17 | 87.99 |
| Sb | 0.3 | 0 | - | - | - | - | - | - | - |
| Ba | 152 | 9 | 289 | 58.79 | 20.36 | 180 | 349 | 169 | 31.03 |
| La | 10.95 | 4 | 135 | 38.89 | 28.91 | 99 | 198 | 99 | 84.94 |
| Ce | 26.8 | 3 | 141 | 19.07 | 13.49 | 116 | 162 | 46 | 68.12 |
| Pr | 3.63 | 1 | 154 | - | - | 154 | 154 | - | - |
| Nd | 18.75 | 1 | 289 | - | - | 289 | 289 | - | - |
| W | 0.01 | 2 | 12.50 | 0.50 | 4.00 | 12 | 13 | 1 | 99.84 |
| Hg | 0.01 | 2 | 8.00 | 2.00 | 25.00 | 6 | 10 | 4 | 99.75 |
| Pb | 4.4 | 7 | 6.86 | 1.13 | 16.40 | 5 | 8 | 3 | 21.83 |
| Bi | 0.01 | 0 | - | - | - | - | - | - | - |
| Th | 1.8 | 4 | 11.25 | 0.83 | 7.37 | 10 | 12 | 2 | 72.41 |
| U | 0.3 | 0 | - | - | - | - | - | - | - |

Notes: *Modified from Morris (2007); conc., concentration; SD, standard deviation; RSD, relative standard deviation ($100 \times (\text{SD}/\text{mean})$); HRD, half relative deviation ($100 \times (\text{certified value} - \text{mean}) / (\text{certified value} + \text{mean})$)

Table 8. Statistics for Olympus Vanta M-Series analyses of pressed powder reference material MW-1^v in standard GeoChem 3-beam mode

| <i>Element</i> | <i>Certified conc. (ppm)</i> | <i>Valid samples</i> | <i>Mean (ppm)</i> | <i>SD (ppm)</i> | <i>RSD (%)</i> | <i>Min. (ppm)</i> | <i>Max. (ppm)</i> | <i>Range (ppm)</i> | <i>HRD (%)</i> |
|----------------|------------------------------|----------------------|-------------------|-----------------|----------------|-------------------|-------------------|--------------------|----------------|
| Mg | 185310 | 9 | 202975 | 3866 | 1.91 | 197621 | 210120 | 12499 | 4.55 |
| Al | 23445 | 9 | 25049 | 345 | 1.38 | 24492 | 25738 | 1246 | 3.31 |
| Si | 190857 | 9 | 190817 | 1944 | 1.02 | 188577 | 194020 | 5443 | 0.01 |
| P | 960.1 | 0 | - | - | - | - | - | - | - |
| S | 0.01 | 0 | - | - | - | - | - | - | - |
| K | 664.1 | 0 | - | - | - | - | - | - | - |
| Ca | 29588 | 9 | 22745 | 234 | 1.03 | 22450 | 23103 | 653 | 13.08 |
| Ti | 1319 | 9 | 1265 | 51.26 | 4.05 | 1182 | 1339 | 157 | 2.07 |
| V | 89 | 7 | 106 | 15.71 | 14.78 | 79 | 125 | 46 | 8.85 |
| Cr | 1920 | 9 | 1848 | 55.57 | 3.01 | 1740 | 1920 | 180 | 1.92 |
| Mn | 1084 | 9 | 1101 | 18.69 | 1.70 | 1067 | 1129 | 62 | 0.79 |
| Fe | 66937 | 9 | 67116 | 267 | 0.40 | 66711 | 67517 | 806 | 0.13 |
| Co | 107 | 9 | 211 | 25.37 | 12.01 | 155 | 247 | 92 | 32.77 |
| Ni | 2214 | 9 | 2111 | 20.25 | 0.96 | 2086 | 2152 | 66 | 2.38 |
| Cu | 41 | 9 | 129 | 5.70 | 4.43 | 118 | 138 | 20 | 51.67 |
| Zn | 59 | 9 | 92.44 | 6.52 | 7.05 | 85 | 108 | 23 | 22.08 |
| As | 2.3 | 0 | - | - | - | - | - | - | - |
| Se | 0.01 | 0 | - | - | - | - | - | - | - |
| Rb | 2.4 | 8 | 2.75 | 0.83 | 30.15 | 2 | 4 | 2 | 6.80 |
| Sr | 11 | 9 | 12.44 | 1.34 | 10.79 | 11 | 15 | 4 | 6.16 |
| Y | 6 | 9 | 5.89 | 0.88 | 14.86 | 5 | 7 | 2 | 0.94 |
| Zr | 11 | 9 | 14.22 | 1.62 | 11.38 | 12 | 18 | 6 | 12.78 |
| Nb | 0.4 | 0 | - | - | - | - | - | - | - |
| Mo | 0.01 | 7 | 7.86 | 1.55 | 19.75 | 5 | 10 | 5 | 99.75 |
| Ag | 0.01 | 0 | - | - | - | - | - | - | - |
| Cd | 0.01 | 0 | - | - | - | - | - | - | - |
| Sn | 0.01 | 6 | 29.33 | 10.16 | 34.64 | 20 | 47 | 27 | 99.93 |
| Sb | 2.5 | 1 | 31.00 | - | - | 31 | 31 | - | - |
| Ba | 24 | 7 | 240 | 76.07 | 31.77 | 76 | 326 | 250 | 81.78 |
| La | 2.1 | 3 | 111 | 35.81 | 32.27 | 73 | 159 | 86 | 96.29 |
| Ce | 2 | 0 | - | - | - | - | - | - | - |
| Pr | 0.3 | 1 | 151 | - | - | 151 | 151 | - | - |
| Nd | 1.5 | 2 | 290 | 64.5 | 22.28 | 225 | 354 | 129 | 98.97 |
| W | 47 | 0 | - | - | - | - | - | - | - |
| Hg | 0.01 | 0 | - | - | - | - | - | - | - |
| Pb | 0.01 | 0 | - | - | - | - | - | - | - |
| Bi | 0.2 | 0 | - | - | - | - | - | - | - |
| Th | 0.01 | 0 | - | - | - | - | - | - | - |
| U | 0.01 | 0 | - | - | - | - | - | - | - |

Notes: ^vGSWA unpublished data, Morris (2009); conc., concentration; SD, standard deviation; RSD, relative standard deviation ($100 \times (\text{SD}/\text{mean})$); HRD, half relative deviation ($100 \times (\text{certified value} - \text{mean}) / (\text{certified value} + \text{mean})$)

Table 9. Statistics for Olympus Vanta M-Series analyses of pressed powder reference material NEWN305^v in standard GeoChem 3-beam mode

| Element | Certified conc. (ppm) | Valid samples | Mean (ppm) | SD (ppm) | RSD (%) | Min. (ppm) | Max. (ppm) | Range (ppm) | HRD (%) |
|---------|-----------------------|---------------|------------|----------|---------|------------|------------|-------------|---------|
| Mg | 301.5 | 0 | - | - | - | - | - | - | - |
| Al | 133051 | 9 | 155101 | 1843 | 1.19 | 152583 | 159129 | 6546 | 7.65 |
| Si | 92273 | 9 | 106490 | 1426 | 1.34 | 104610 | 109922 | 5312 | 7.15 |
| P | 174.6 | 0 | - | - | - | - | - | - | - |
| S | 899 | 9 | 498 | 39.37 | 7.91 | 424 | 551 | 127 | 28.74 |
| K | 249 | 0 | - | - | - | - | - | - | - |
| Ca | 214.4 | 9 | 164 | 32.67 | 19.94 | 115 | 228 | 113 | 13.35 |
| Ti | 13367 | 9 | 7793 | 75.54 | 0.97 | 7649 | 7898 | 249 | 26.34 |
| V | 472 | 9 | 650 | 19.25 | 2.96 | 619 | 691 | 72 | 15.88 |
| Cr | 3225 | 9 | 2072 | 29.30 | 1.41 | 2035 | 2121 | 86 | 21.76 |
| Mn | 154.9 | 9 | 179 | 24.00 | 13.39 | 127 | 212 | 85 | 7.28 |
| Fe | 268868 | 9 | 218573 | 840 | 0.38 | 217141 | 219615 | 2474 | 10.32 |
| Co | 28 | 9 | 286 | 55.32 | 19.31 | 179 | 397 | 218 | 82.19 |
| Ni | 314 | 9 | 171 | 8.79 | 5.15 | 160 | 189 | 29 | 29.57 |
| Cu | 1036 | 9 | 641 | 9.13 | 1.42 | 632 | 663 | 31 | 23.53 |
| Zn | 111 | 9 | 54.00 | 5.40 | 9.99 | 45 | 62 | 17 | 34.55 |
| As | 52 | 9 | 23.67 | 2.79 | 11.78 | 19 | 28 | 9 | 37.44 |
| Se | 1.3 | 6 | 5.00 | 1.00 | 20.00 | 4 | 7 | 3 | 58.73 |
| Rb | 6 | 0 | - | - | - | - | - | - | - |
| Sr | 4 | 0 | - | - | - | - | - | - | - |
| Y | 5 | 6 | 5.17 | 1.07 | 20.66 | 4 | 7 | 3 | 1.64 |
| Zr | 146 | 9 | 153.60 | 15.37 | 10.01 | 140 | 194 | 54 | 2.52 |
| Nb | 6 | 0 | - | - | - | - | - | - | - |
| Mo | 4 | 9 | 17.44 | 2.11 | 12.12 | 14 | 20 | 6 | 62.69 |
| Ag | 0.01 | 0 | - | - | - | - | - | - | - |
| Cd | 0.01 | 0 | - | - | - | - | - | - | - |
| Sn | 2 | 7 | 40.00 | 7.39 | 18.47 | 26 | 49 | 23 | 90.48 |
| Sb | 2.6 | 3 | 48.33 | 13.57 | 28.08 | 33 | 66 | 33 | 89.79 |
| Ba | 22 | 8 | 106 | 18.34 | 17.31 | 83 | 130 | 47 | 65.63 |
| La | 2 | 3 | 130 | 20.53 | 15.83 | 110 | 158 | 48 | 96.96 |
| Ce | 8 | 3 | 167 | 17.02 | 10.17 | 149 | 190 | 41 | 90.87 |
| Pr | 0.01 | 1 | 281 | - | - | 281 | 281 | - | - |
| Nd | 0.01 | 1 | 506 | - | - | 506 | 506 | - | - |
| W | 0.01 | 0 | - | - | - | - | - | - | - |
| Hg | 35 | 0 | - | - | - | - | - | - | - |
| Pb | 16 | 0 | - | - | - | - | - | - | - |
| Bi | 0.6 | 9 | 53.67 | 8.54 | 15.91 | 37 | 68 | 31 | 97.79 |
| Th | 14 | 5 | 13.20 | 2.79 | 21.10 | 10 | 17 | 7 | 2.94 |
| U | 3 | 8 | 7.25 | 0.66 | 9.12 | 6 | 8 | 2 | 41.46 |

Notes: ^vGSWA unpublished data, Morris (2009); conc., concentration; SD, standard deviation; RSD, relative standard deviation ($100 \times (\text{SD}/\text{mean})$); HRD, half relative deviation ($100 \times (\text{certified value} - \text{mean}) / (\text{certified value} + \text{mean})$)

Table 10. Statistics for Olympus Vanta M-Series analyses of pressed powder reference material BIR-1a^a in standard GeoChem 3-beam mode

| Element | Certified conc. (ppm) | Valid samples | Mean (ppm) | SD (ppm) | RSD (%) | Min. (ppm) | Max. (ppm) | Range (ppm) | HRD (%) |
|---------|-----------------------|---------------|------------|----------|---------|------------|------------|-------------|---------|
| Mg | 58494 | 9 | 36478 | 1782 | 4.88 | 33603 | 40409 | 6806 | 23.18 |
| Al | 82032 | 9 | 96026 | 1280 | 1.33 | 93794 | 97838 | 4044 | 7.86 |
| Si | 224186 | 9 | 209661 | 2247 | 1.07 | 205488 | 212756 | 7268 | 3.35 |
| P | 91.65 | 0 | - | - | - | - | - | - | - |
| S | 0.01 | 0 | - | - | - | - | - | - | - |
| K | 249 | 0 | - | - | - | - | - | - | - |
| Ca | 95054 | 9 | 90491 | 631 | 0.70 | 89659 | 91907 | 2248 | 2.46 |
| Ti | 5754 | 9 | 5855 | 147 | 2.51 | 5546 | 6029 | 483 | 0.86 |
| V | 310 | 9 | 354 | 37.07 | 10.47 | 279 | 420 | 141 | 6.64 |
| Cr | 370 | 9 | 290 | 9.98 | 3.44 | 271 | 307 | 36 | 12.14 |
| Mn | 1355 | 9 | 1217 | 19.29 | 1.59 | 1184 | 1247 | 63 | 5.39 |
| Fe | 79038 | 9 | 76162 | 186 | 0.24 | 75789 | 76464 | 675 | 1.85 |
| Co | 52 | 9 | 176 | 39.29 | 22.31 | 128 | 252 | 124 | 54.41 |
| Ni | 170 | 9 | 181 | 5.54 | 3.05 | 172 | 190 | 18 | 3.26 |
| Cu | 125 | 9 | 137 | 5.31 | 3.86 | 130 | 148 | 18 | 4.82 |
| Zn | 70 | 9 | 68.56 | 4.03 | 5.88 | 61 | 75 | 14 | 1.04 |
| As | 0.44 | 0 | - | - | - | - | - | - | - |
| Se | 0.01 | 0 | - | - | - | - | - | - | - |
| Rb | 0.01 | 0 | - | - | - | - | - | - | - |
| Sr | 110 | 9 | 109 | 1.64 | 1.51 | 106 | 111 | 5 | 0.66 |
| Y | 16 | 9 | 17.11 | 0.57 | 3.31 | 16 | 18 | 2 | 3.36 |
| Zr | 18 | 9 | 15.67 | 1.49 | 9.52 | 13 | 18 | 5 | 6.93 |
| Nb | 0.6 | 0 | - | - | - | - | - | - | - |
| Mo | 0.01 | 4 | 7.00 | 0.71 | 10.10 | 6 | 8 | 2 | 99.71 |
| Ag | 0.01 | 1 | 7.00 | - | - | 7 | 7 | - | - |
| Cd | 0.01 | 4 | 22.00 | 3.16 | 14.37 | 18 | 26 | 8 | 99.91 |
| Sn | 0.01 | 8 | 32.00 | 10.34 | 32.33 | 21 | 55 | 34 | 99.94 |
| Sb | 0.58 | 1 | 57.00 | - | - | 57 | 57 | - | - |
| Ba | 7 | 6 | 105 | 25.66 | 24.52 | 80 | 158 | 78 | 87.46 |
| La | 0.63 | 1 | 158 | - | - | 158 | 158 | - | - |
| Ce | 1.9 | 1 | 197 | - | - | 197 | 197 | - | - |
| Pr | 0.01 | 1 | 165 | - | - | 165 | 165 | - | - |
| Nd | 0.01 | 0 | - | - | - | - | - | - | - |
| W | 0.01 | 2 | 10.00 | 0.00 | 0.00 | 10 | 10 | 0 | 99.80 |
| Hg | 0.01 | 3 | 6.33 | 1.89 | 29.77 | 5 | 9 | 4 | 99.68 |
| Pb | 3 | 6 | 5.00 | 1.53 | 30.55 | 4 | 8 | 4 | 25.00 |
| Bi | 0.01 | 0 | - | - | - | - | - | - | - |
| Th | 0.01 | 6 | 11.17 | 1.07 | 9.56 | 10 | 13 | 3 | 99.82 |
| U | 0.01 | 0 | - | - | - | - | - | - | - |

Notes: ^aModified from Fluxana (2015); conc., concentration; SD, standard deviation; RSD, relative standard deviation ($100 \times (\text{SD}/\text{mean})$); HRD, half relative deviation ($(100 \times (\text{certified value} - \text{mean}) / (\text{certified value} + \text{mean}))$)

Table 11. Statistics for Olympus Vanta M-Series analyses of pressed powder reference material W-2^a in standard GeoChem 3-beam mode

| Element | Certified conc. (ppm) | Valid samples | Mean (ppm) | SD (ppm) | RSD (%) | Min. (ppm) | Max. (ppm) | Range (ppm) | HRD (%) |
|---------|-----------------------|---------------|------------|----------|---------|------------|------------|-------------|---------|
| Mg | 38413 | 9 | 27734 | 1070 | 3.86 | 25990 | 28803 | 2813 | 16.14 |
| Al | 81768 | 9 | 89682 | 1158 | 1.29 | 87949 | 91375 | 3426 | 4.62 |
| Si | 246249 | 9 | 239194 | 1940 | 0.81 | 236284 | 242487 | 6203 | 1.45 |
| P | 611 | 9 | 437 | 33.68 | 7.70 | 388 | 497 | 109 | 16.55 |
| S | 79 | 0 | - | - | - | - | - | - | - |
| K | 5197 | 9 | 4471 | 60.93 | 1.36 | 4400 | 4572 | 172 | 7.51 |
| Ca | 77616 | 9 | 75503 | 356 | 0.47 | 74852 | 76002 | 1150 | 1.38 |
| Ti | 6354 | 9 | 6601 | 149 | 2.25 | 6358 | 6897 | 539 | 1.91 |
| V | 260 | 9 | 315 | 29.33 | 9.30 | 261 | 350 | 89 | 9.62 |
| Cr | 92 | 9 | 85.00 | 10.35 | 12.18 | 69 | 103 | 34 | 3.96 |
| Mn | 1293 | 9 | 1160 | 21.65 | 1.87 | 1137 | 1208 | 71 | 5.43 |
| Fe | 75750 | 9 | 73310 | 329 | 0.45 | 72905 | 73898 | 993 | 1.64 |
| Co | 43 | 7 | 171 | 41.73 | 24.38 | 94 | 219 | 125 | 59.84 |
| Ni | 70 | 9 | 84.33 | 3.94 | 4.68 | 78 | 92 | 14 | 9.29 |
| Cu | 110 | 9 | 115 | 5.02 | 4.36 | 107 | 123 | 16 | 2.27 |
| Zn | 80 | 9 | 77.78 | 4.24 | 5.45 | 74 | 88 | 14 | 1.41 |
| As | 1.20 | 1 | 5.00 | - | - | 5 | 5 | - | - |
| Se | 0.01 | 1 | 3.00 | - | - | 3 | 3 | - | - |
| Rb | 21 | 9 | 20.11 | 1.37 | 6.81 | 18 | 23 | 5 | 2.16 |
| Sr | 190 | 9 | 194 | 1.52 | 0.79 | 191 | 196 | 5 | 1.07 |
| Y | 23 | 9 | 22.89 | 1.29 | 5.62 | 21 | 24 | 3 | 0.24 |
| Zr | 100 | 9 | 91.56 | 1.71 | 1.86 | 89 | 95 | 6 | 4.41 |
| Nb | 7.9 | 1 | 4.00 | - | - | 4 | 4 | - | - |
| Mo | 0.01 | 6 | 6.83 | 1.77 | 25.93 | 4 | 9 | 5 | 99.71 |
| Ag | 0.01 | 0 | - | - | - | - | - | - | - |
| Cd | 0.01 | 4 | 23.50 | 10.16 | 43.24 | 16 | 41 | 25 | 99.91 |
| Sn | 0.01 | 6 | 32.83 | 5.87 | 17.88 | 25 | 41 | 16 | 99.94 |
| Sb | 0.79 | 0 | - | - | - | - | - | - | - |
| Ba | 170 | 9 | 286 | 39.61 | 13.87 | 202 | 345 | 143 | 25.37 |
| La | 10 | 4 | 133 | 15.41 | 11.59 | 107 | 145 | 38 | 86.01 |
| Ce | 23 | 3 | 186 | 43.61 | 23.49 | 124 | 217 | 93 | 77.96 |
| Pr | 0.01 | 2 | 251 | 23.00 | 9.16 | 228 | 274 | 46 | 99.99 |
| Nd | 13 | 3 | 293 | 88.64 | 30.29 | 228 | 418 | 190 | 91.49 |
| W | 0.01 | 3 | 12.67 | 0.94 | 7.44 | 12 | 14 | 2 | 99.84 |
| Hg | 0.01 | 1 | 6.00 | - | - | 6 | 6 | - | - |
| Pb | 9.3 | 8 | 11.75 | 0.83 | 7.06 | 11 | 13 | 2 | 11.64 |
| Bi | 0.01 | 0 | - | - | - | - | - | - | - |
| Th | 2.4 | 7 | 12.57 | 1.99 | 15.83 | 10 | 16 | 6 | 67.94 |
| U | 0.01 | 0 | - | - | - | - | - | - | - |

Notes: ^aModified from Fluxana (2015); conc., concentration; SD, standard deviation; RSD, relative standard deviation ($100 \times (\text{SD}/\text{mean})$); HRD, half relative deviation ($(100 \times (\text{certified value} - \text{mean}) / (\text{certified value} + \text{mean}))$)

Table 12. Statistics for Olympus Vanta M-Series analyses of pressed powder reference material TILL-1^A in standard GeoChem 3-beam mode

| Element | Certified conc. (ppm) | Valid samples | Mean (ppm) | SD (ppm) | RSD (%) | Min. (ppm) | Max. (ppm) | Range (ppm) | HRD (%) |
|---------|-----------------------|---------------|------------|----------|---------|------------|------------|-------------|---------|
| Mg | 12965 | 9 | 11457 | 1137 | 9.92 | 8690 | 13253 | 4563 | 6.18 |
| Al | 72506 | 9 | 72812 | 854 | 1.17 | 71005 | 73666 | 2661 | 0.21 |
| Si | 284673 | 9 | 269293 | 2088 | 0.78 | 266173 | 272563 | 6390 | 2.78 |
| P | 960.1 | 9 | 1185 | 46.44 | 3.92 | 1096 | 1240 | 144 | 10.50 |
| S | 0.01 | 0 | - | - | - | - | - | - | - |
| K | 18429 | 9 | 15743 | 108 | 0.68 | 15564 | 15867 | 303 | 7.86 |
| Ca | 19440 | 9 | 17417 | 92.25 | 0.53 | 17263 | 17535 | 272 | 5.49 |
| Ti | 5874 | 9 | 5929 | 187 | 3.15 | 5776 | 6362 | 586 | 0.47 |
| V | 99 | 6 | 129 | 15.47 | 11.98 | 119 | 163 | 44 | 13.22 |
| Cr | 65 | 9 | 86.67 | 13.18 | 15.21 | 67 | 113 | 46 | 14.29 |
| Mn | 1394 | 9 | 1342 | 21.65 | 1.61 | 1312 | 1377 | 65 | 1.92 |
| Fe | 47702 | 9 | 46761 | 322 | 0.69 | 46257 | 47224 | 967 | 1.00 |
| Co | 18 | 5 | 82.50 | 38.58 | 46.77 | 0 | 118 | 118 | 64.18 |
| Ni | 24 | 9 | 35.00 | 1.76 | 5.04 | 33 | 38 | 5 | 18.64 |
| Cu | 47 | 9 | 51.67 | 5.01 | 9.67 | 40 | 57 | 17 | 4.73 |
| Zn | 98 | 9 | 97.67 | 3.59 | 3.68 | 94 | 104 | 10 | 0.17 |
| As | 18 | 9 | 20.00 | 1.49 | 7.45 | 18 | 23 | 5 | 5.26 |
| Se | 0.01 | 0 | - | - | - | - | - | - | - |
| Rb | 44 | 9 | 43.22 | 0.79 | 1.82 | 42 | 45 | 3 | 0.89 |
| Sr | 291 | 9 | 296 | 2.20 | 0.74 | 292 | 300 | 8 | 0.81 |
| Y | 38 | 9 | 34.89 | 1.10 | 3.15 | 33 | 36 | 3 | 4.27 |
| Zr | 502 | 9 | 460 | 4.37 | 0.95 | 454 | 467 | 13 | 4.45 |
| Nb | 10 | 9 | 6.22 | 0.79 | 12.63 | 5 | 7 | 2 | 23.29 |
| Mo | 2 | 9 | 8.78 | 1.03 | 11.74 | 7 | 11 | 4 | 62.89 |
| Ag | 0.01 | 0 | - | - | - | - | - | - | - |
| Cd | 0.01 | 0 | - | - | - | - | - | - | - |
| Sn | 0.01 | 6 | 28.83 | 7.06 | 24.48 | 17 | 39 | 22 | 99.93 |
| Sb | 0.01 | 1 | 31.00 | - | - | 31 | 31 | - | - |
| Ba | 702 | 9 | 890 | 59.14 | 6.64 | 805 | 973 | 168 | 11.82 |
| La | 28 | 1 | 96.00 | - | - | 96 | 96 | - | - |
| Ce | 71 | 6 | 155 | 34.82 | 22.42 | 102 | 210 | 108 | 37.26 |
| Pr | 0.01 | 1 | 166 | - | - | 166 | 166 | - | - |
| Nd | 26 | 2 | 235 | 30.50 | 13.01 | 204 | 265 | 61 | 80.04 |
| W | 0.01 | 0 | - | - | - | - | - | - | - |
| Hg | 0.01 | 1 | 4.00 | - | - | 4 | 4 | - | - |
| Pb | 22 | 9 | 22.11 | 1.45 | 6.55 | 20 | 24 | 4 | 0.25 |
| Bi | 0.01 | 0 | - | - | - | - | - | - | - |
| Th | 5.6 | 0 | - | - | - | - | - | - | - |
| U | 2.2 | 0 | - | - | - | - | - | - | - |

Notes: ^AModified from Fluxana (2015); conc., concentration; SD, standard deviation; RSD, relative standard deviation ($100 \times (\text{SD}/\text{mean})$); HRD, half relative deviation ($(100 \times (\text{certified value} - \text{mean}) / (\text{certified value} + \text{mean}))$)

Table 13. Statistics for Olympus Vanta M-Series analyses of pressed powder reference material STSD-4^a in standard GeoChem 3-beam mode

| Element | Certified conc. (ppm) | Valid samples | Mean (ppm) | SD (ppm) | RSD (%) | Min. (ppm) | Max. (ppm) | Range (ppm) | HRD (%) |
|---------|-----------------------|---------------|------------|----------|---------|------------|------------|-------------|---------|
| Mg | 12664 | 9 | 12344 | 1391 | 11.27 | 10359 | 15518 | 5159 | 1.28 |
| Al | 64038 | 9 | 60354 | 1106 | 1.83 | 58013 | 62056 | 4043 | 2.96 |
| Si | 275324 | 9 | 253674 | 4139 | 1.63 | 246650 | 259000 | 12350 | 4.09 |
| P | 872.8 | 9 | 1046 | 43.06 | 4.12 | 996 | 1103 | 107 | 9.02 |
| S | 900 | 9 | 983 | 81.62 | 8.30 | 872 | 1169 | 297 | 4.41 |
| K | 13282 | 9 | 11599 | 148 | 1.27 | 11335 | 11811 | 476 | 6.77 |
| Ca | 28588 | 9 | 28056 | 284 | 1.01 | 27617 | 28512 | 895 | 0.94 |
| Ti | 1199 | 9 | 4216 | 94.94 | 2.25 | 4066 | 4346 | 280 | 55.72 |
| V | 106 | 3 | 103 | 7.79 | 7.56 | 97 | 114 | 17 | 1.44 |
| Cr | 93 | 9 | 111 | 17.43 | 15.75 | 74 | 140 | 66 | 8.67 |
| Mn | 1549 | 9 | 1428 | 19.81 | 1.39 | 1401 | 1461 | 60 | 4.07 |
| Fe | 39869 | 9 | 37933 | 209 | 0.55 | 37482 | 38177 | 695 | 2.49 |
| Co | 13 | 2 | 25.60 | 31.99 | 125 | 0 | 74 | 74 | 32.64 |
| Ni | 30 | 9 | 40.89 | 3.51 | 8.59 | 36 | 47 | 11 | 15.36 |
| Cu | 65 | 9 | 72.56 | 2.46 | 3.38 | 67 | 76 | 9 | 5.49 |
| Zn | 107 | 9 | 105 | 2.54 | 2.43 | 102 | 109 | 7 | 1.10 |
| As | 15 | 9 | 15.11 | 1.20 | 7.92 | 14 | 17 | 3 | 0.37 |
| Se | 0.01 | 0 | - | - | - | - | - | - | - |
| Rb | 39 | 9 | 36.33 | 1.05 | 2.90 | 35 | 38 | 3 | 3.54 |
| Sr | 350 | 9 | 360 | 2.20 | 0.61 | 356 | 363 | 7 | 1.44 |
| Y | 24 | 9 | 24.78 | 1.69 | 6.80 | 23 | 27 | 4 | 1.60 |
| Zr | 190 | 9 | 160 | 10.39 | 6.48 | 147 | 177 | 30 | 8.47 |
| Nb | 9 | 3 | 3.00 | 0.82 | 27.22 | 2 | 4 | 2 | 50.00 |
| Mo | 5 | 9 | 7.78 | 2.35 | 30.17 | 5 | 13 | 8 | 21.74 |
| Ag | 0.01 | 0 | - | - | - | - | - | - | - |
| Cd | 0.01 | 0 | - | - | - | - | - | - | - |
| Sn | 2 | 4 | 23.50 | 4.92 | 20.96 | 20 | 32 | 12 | 84.31 |
| Sb | 7.3 | 0 | - | - | - | - | - | - | - |
| Ba | 2000 | 9 | 2207 | 80.56 | 3.65 | 2062 | 2325 | 263 | 4.91 |
| La | 24 | 3 | 111 | 27.98 | 25.13 | 82 | 149 | 67 | 64.53 |
| Ce | 44 | 4 | 126 | 30.12 | 24.00 | 95 | 169 | 74 | 48.08 |
| Pr | 0.01 | 1 | 155 | - | - | 155 | 155 | - | - |
| Nd | 21 | 2 | 336 | 56.50 | 16.84 | 279 | 392 | 113 | 88.22 |
| W | 0.01 | 0 | - | - | - | - | - | - | - |
| Hg | 0.01 | 1 | 5.00 | - | - | 5 | 5 | - | - |
| Pb | 16 | 9 | 18.11 | 1.66 | 9.18 | 16 | 21 | 5 | 6.19 |
| Bi | 0.01 | 0 | - | - | - | - | - | - | - |
| Th | 4.3 | 0 | - | - | - | - | - | - | - |
| U | 3 | 0 | - | - | - | - | - | - | - |

Notes: ^aModified from Fluxana (2015); conc., concentration; SD, standard deviation; RSD, relative standard deviation ($100 \times (\text{SD}/\text{mean})$); HRD, half relative deviation ($(100 \times (\text{certified value} - \text{mean}) / (\text{certified value} + \text{mean}))$)

Count times

As discussed by Morris (2009), it is important to optimize the count time to ensure a balance between instrument precision and sampling intensity. Increased measurement times improve counting statistics and reduce uncertainty, although this simultaneously reduces the number of samples that can be collected within a set time. Measurements were made in the GeoChem mode using beam collection times of 10, 20, and 30 seconds, respectively, to test typical fast-sampling times for the instrument and observe the impact of beam-time variation on accuracy and precision.

Correlation with certified values is generally not observed to improve significantly beyond count times of 10 seconds, although Zn shows an improvement in fit correlation from approximately 0.7 (R^2) to 0.8 (R^2) with count time increasing from 10 seconds to 30 seconds. Phosphorus had the worst calibration of the various elements tested, although the required calibration factor did not change with varying count time. Improvements in the correlations with certified values improve with increasing count times for Ni, Cu, Zn, and Pb, although these elements have low concentrations in all the measured standards.

The results support using shorter count times with the Olympus Vanta, although improvements in precision and uncertainty can be achieved with longer count times, if required. Calibration factors and correlation with certified values, generally did not improve significantly beyond count times of 10 seconds per beam, suggesting that longer count times may not be necessary for general uses. However, an increased count time of 20–30 seconds for beam 1 resulted in improved measurements of Ni, Cu, Zn, and Pb, which can be critical in accurate measurement of rocks with potential economic mineralization, although not of significant value in general geological applications. Therefore, a count time of 20 seconds for beam 1 (from Ti to U) and 10 seconds for the remaining beams has been adopted by the GSWA for general measurements.

Grain size

Sample inhomogeneity and surface conditions have the potential to significantly impact pXRF precision and accuracy due to the small analytical area (8 mm) and minimal sample preparation required for this technique, particularly in comparison to laboratory-based XRF analysis typically conducted on pressed bulk powder samples (Morris, 2009). Core-cleaning and preparation requirements for HyLogger spectral scanning (Hancock and Huntington, 2010) minimize the potential impact of surface conditions on complementary pXRF measurements. Testing by Morris (2009) indicated that surface morphology has a smaller effect than sample homogeneity; hence, the assumption that grain size can have the largest impact on analytical precision on the relatively smooth surface of cleaned diamond drillcore. Conversely, the angular surfaces of broken core and drill chips can be analysed with high precision, using multiple measurements of various flat pieces fitted under the 8-mm window of the pXRF instrument.

Measurements of typical fresh coarse-grained rock were collected with the Olympus Vanta to investigate the magnitude of this effect and its potential to bias geochemical trends and affect the reproducibility of data. Eighteen measurements were collected at random locations on hand specimen

GSWA 201965 (Fig. 5), a very coarse-grained (>15 mm) granitic pegmatite composed mainly of quartz, spodumene, and minor zeolites from the Greenbushes Li deposit in the South West Terrane of the Yilgarn Craton (Wawryk and Hancock, 2019). Seven measurements (Fig. 6) were collected at random locations on a coarse-grained (5–7 mm) igneous intrusion in the Jimberlana dyke, composed of plagioclase, pyroxene, chlorite, white mica, and minor quartz from a 215-m depth in drillcore 18JBDD002, a Cu-Ni exploration core drilled by AusQuest in 2018.

A comparison of the results against previous measurements of the felsic pressed pellet CRM KG-1 clearly demonstrate that the precision of pXRF measurements improves with reduced grain size (Tables 14, 15). The precision and reproducibility of measurements for elements with concentrations significantly above the LOQ were weakest on the coarsest pegmatite sample GSWA 201965 with RSD typically >25% (Fig. 7a). By comparison, precision on the relatively finer-grained 18JBDD002 core sample was significantly improved with RSD <15% and commonly <5% for most reliably detectable elements, and further improved on the homogenous pressed pellet KG-1 with RSD <10% and commonly <1% (Fig. 7b,c). This general trend of improved precision with reduced grain size was observed regardless of whether elemental abundances between samples were comparable (e.g. Al, Si) or dissimilar (e.g. Fe, K).

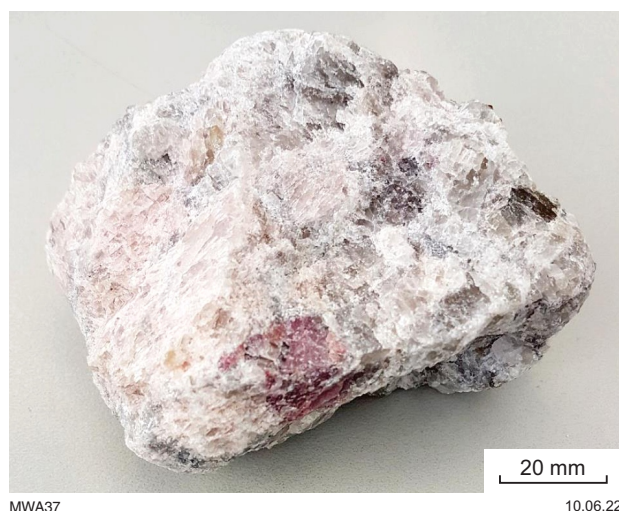


Figure 5. Greenbushes Li deposit pegmatite specimen GSWA 201965 composed of very coarse-grained (>15 mm) quartz, spodumene, and minor zeolites



Figure 6. Coarse-grained (5–7 mm) intermediate igneous intrusion from 215 m in drillcore 18JBDD002 (M0002838) from the Jimberlana dyke intrusion, composed primarily of plagioclase, pyroxene, chlorite, white mica, and minor quartz

These results may be due to the reduction in relative sample homogeneity as average grain size approaches or exceeds the measurement area of the pXRF (8 mm), increasing the potential for individual mineral grains to dominate and bias the measured chemistry. A similar effect is likely to be observed in samples with significant mineral segregation (e.g. gneisses and finely interlayered sedimentary rocks) with increasingly larger zonation, leading to reduced textural homogeneity at the scale of the measurement. Accurate measurement of very coarse-grained-material (>10 mm) will require multiple measurements on various spots, to achieve representative statistics. However, the precision of measurements on the coarse-grained intrusive sample is well within acceptable limits for the purpose of collecting general reconnaissance geochemical data, indicating that single measurements can provide accurate representative results for coarse-grained samples (>5 mm) too.

Sampling intervals

As part of a pilot study collecting complementary geochemical data for HyLogger-3 downhole mineral logs, additional pXRF measurements were collected at regular intervals along the Jimberlana dyke drillcore 18JBDD002 (Fig. 8). Using the Olympus Vanta once per tray, at a constant position of 10 cm from the start of the tray, approximately one measurement per 4–5 m, factory-calibrated pXRF measurements were collected. Extra measurements were collected about once per tray channel for the interval 189–282 m, to collect a representative sample of higher-density measurements. The pXRF measurements were subsequently imported as scalars into the corresponding HyLogger dataset and manually appended to co-located spectral measurements.

Drillcore 18JBDD002 was previously assayed by AusQuest at approximately 4–5-m intervals by inductively coupled plasma mass spectrometry (ICP-MS) using multi-acid partial digests of 20-cm half-core samples (assay data from WAMEX Report A118977; AusQuest Limited, 2019). The comparable sampling densities and elemental suites between the pXRF and ICP-MS assays support direct comparison of relative accuracy and precision with the measurements using the GSWA Olympus Vanta. Comparative downhole plots show good correlation for elements above the LOQ, notably Mg, Ca, Ti, Fe, Ni, Cu, Sr, and Zr, with accurate concentrations and reproduction of geochemical trends (Figs 9a,c–e,g–j). Concentrations of Co and Al from pXRF measurements are overestimated compared to the ICP-MS results, although comparable geochemical trends are still observed downhole, and calibration could be improved with user factors (Figs 9b,f).

Elements with abundances below LOQ, such as La and Th, are inconsistently detected (Figs 9k,l), requiring a more sensitive technique to accurately observe downhole trends. When detected, the abundances of these trace elements are overestimated compared to the ICP-MS results, likely due to calibration errors expected for elemental concentrations below LOQ, instrument noise or sample inhomogeneity (e.g. nugget effect). The low-resolution sampling resulted in some narrow anomalies being missed by the pXRF assay, such as the elevated Zr concentration >100 ppm at 49 m depth in the ICP-MS assay (Fig. 9j). Smaller sampling volumes also resulted in increased scatter and apparent anomalies compared to the ICP-MS results, such as overestimated Mg measurements at 122–132 m depth (Fig. 9a).

Higher sampling density is not observed to significantly improve accuracy or elucidate trends, instead highlighting the increased scatter of the pXRF results. This can be attributed to the lower homogeneity of the sampled core at the scale of the pXRF measurement area, in comparison to the bulk sampling and homogenization employed during ICP-MS analysis. Increased sampling density is likely to improve collection and representation of finer-scale geological features and geochemical trends that may otherwise be missed (e.g. veining, cyclicity in sediments), and reduce the apparent impact of outliers, although this is at the expense of greater dispersion in large-scale geochemical trends. However, the lower sampling density of a single pXRF shot per tray appears to be sufficient to observe broad downhole geochemical trends, minimize analytical time requirements, and enable simpler incorporation into HyLogger scanning workflows.

Comparison with other methods

Minalyzer CS – XRF core scanner

High-resolution downhole geochemistry was subsequently collected on drillcore 18JBDD002 to 227 m depth, using a Minalyzer CS continuous XRF core scanner (Mo-anode operated at 23 kV/23 µA) at the CSIRO Australian Resources Research Centre in Kensington, Perth. Data were collected from a 10-mm beam area moving along the core at 10 mm/s, and binned to 10-cm and 1-m sections for improved readability and signal-to-noise ratios. Multiple 20-cm half-core sections were independently measured using a PANalytical MagiX FAST XRF (Rh-anode, 4 kW tube) and the GSWA Vanta and compared against the respective Minalyzer results (Tables 16–18). Calibration plots confirm good correlation between the three techniques for most elements (Figs 10a–f), with the exception of poor precision for Si from the Minalyzer (Fig. 10c). Improved comparative accuracy and lower LODs for several elements (e.g. Zr) from the Vanta are likely due to the shorter collection time utilized by the Minalyzer instrument.

Comparative downhole plots of Minalyzer data show good correlation with the ICP-MS results for most elements, including Mg, Ca, Ti, Cu, and Sr (Figs 11a,c,d,g,h), with accurate concentrations and reproductions of geochemical trends. Abundances of several elements such as Al, Fe, Ni, and Zr are over- or underestimated by the Minalyzer (Fig. 11b,e,f,i), although the respective downhole geochemical trends are accurately replicated. The greater sampling density of the Minalyzer analysis enabled the capture of narrow geochemical features missed by the broader pXRF assay, including the elevated Cu anomaly at 49 m depth, and elevated Ni concentrations at 137 m and 147 m depth. However, a sharp discordance in downhole trends for all elements at 222 m, inconsistent with the pXRF and ICP-MS measurements, suggests an instrumental stability issue encountered by the Minalyzer during analysis.

Similar to pXRF results, Minalyzer measurements show significant dispersion compared to the homogenized ICP-MS samples and elements below LOQ are sporadically detected and overestimated (e.g. Pb, Fig. 11j). The most likely reasons for this are greater sample density and smaller sample areas analysed by the Minalyzer, which accurately represent the relative inhomogeneity and variability of the core.

Table 14. Statistics for Olympus Vanta M-Series analyses in standard GeoChem 3-beam mode for coarse-grained rock sample GSWA 2019656

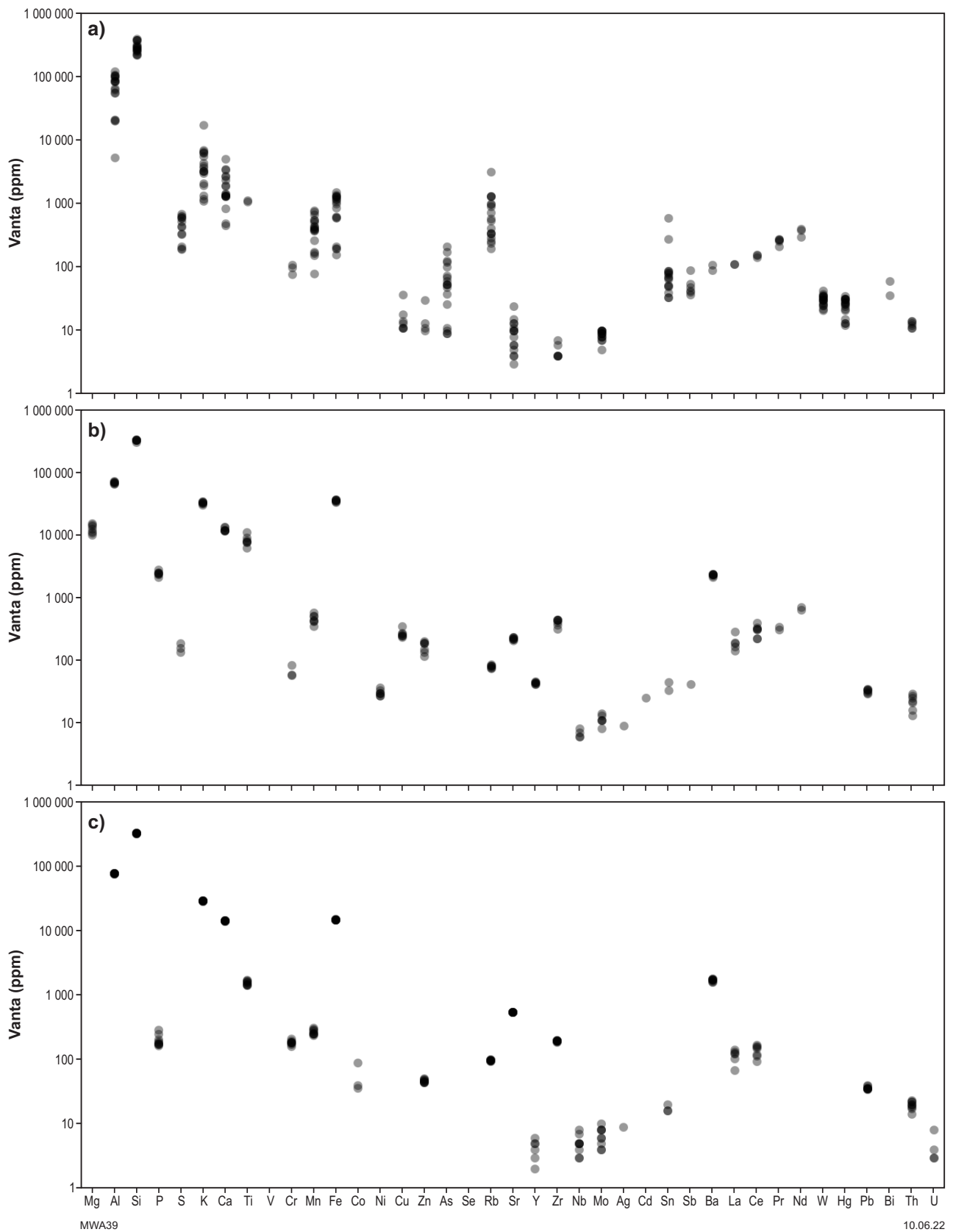
| <i>Element</i> | <i>Valid Samples</i> | <i>Mean (ppm)</i> | <i>SD (ppm)</i> | <i>RSD (%)</i> | <i>Min. (ppm)</i> | <i>Max. (ppm)</i> | <i>Range (ppm)</i> |
|----------------|----------------------|-------------------|-----------------|----------------|-------------------|-------------------|--------------------|
| Mg | 0 | - | - | - | - | - | - |
| Al | 18 | 71483 | 34176 | 47.81 | 5294 | 121642 | 116348 |
| Si | 18 | 294972 | 54485 | 18.47 | 217970 | 395242 | 177272 |
| P | 0 | - | - | - | - | - | - |
| S | 13 | 4456 | 173 | 38.79 | 193 | 693 | 500 |
| K | 18 | 4540 | 3658 | 80.56 | 1097 | 17513 | 16416 |
| Ca | 18 | 1942 | 1158 | 59.61 | 457 | 5132 | 4675 |
| Ti | 2 | 1103 | 33.50 | 3.04 | 1069 | 1136 | 67 |
| V | 0 | - | - | - | - | - | - |
| Cr | 3 | 94.00 | 13.37 | 14.22 | 76 | 108 | 32 |
| Mn | 18 | 414 | 194 | 46.90 | 78 | 776 | 698 |
| Fe | 18 | 886 | 453 | 51.17 | 158 | 1517 | 1359 |
| Co | 0 | - | - | - | - | - | - |
| Ni | 0 | - | - | - | - | - | - |
| Cu | 7 | 16.43 | 8.72 | 53.05 | 11 | 37 | 26 |
| Zn | 4 | 16.00 | 8.16 | 50.97 | 10 | 30 | 20 |
| As | 18 | 68.94 | 55.52 | 80.53 | 9 | 210 | 201 |
| Se | 0 | - | - | - | - | - | - |
| Rb | 18 | 788 | 685 | 86.89 | 196 | 3143 | 2947 |
| Sr | 15 | 9.47 | 5.28 | 55.75 | 3 | 24 | 21 |
| Y | 0 | - | - | - | - | - | - |
| Zr | 6 | 4.83 | 1.21 | 25.10 | 4 | 7 | 3 |
| Nb | 0 | - | - | - | - | - | - |
| Mo | 15 | 8.60 | 1.41 | 16.33 | 5 | 10 | 5 |
| Ag | 0 | - | - | - | - | - | - |
| Cd | 0 | - | - | - | - | - | - |
| Sn | 16 | 109 | 136 | 125 | 33 | 591 | 558 |
| Sb | 6 | 52.17 | 17.42 | 33.39 | 37 | 89 | 52 |
| Ba | 2 | 99.50 | 9.50 | 9.55 | 90 | 109 | 19 |
| La | 2 | 111 | 0.00 | 0.00 | 111 | 111 | 0 |
| Ce | 3 | 151 | 5.72 | 3.79 | 143 | 156 | 13 |
| Pr | 5 | 257 | 24.05 | 9.36 | 210 | 276 | 66 |
| Nd | 3 | 360 | 42.43 | 11.79 | 301 | 399 | 98 |
| W | 18 | 30.72 | 5.58 | 18.15 | 21 | 43 | 22 |
| Hg | 18 | 24.89 | 7.18 | 28.85 | 12 | 35 | 23 |
| Pb | 0 | - | - | - | - | - | - |
| Bi | 2 | 48.00 | 12.00 | 25.00 | 36 | 60 | 24 |
| Th | 6 | 12.50 | 1.26 | 10.07 | 11 | 14 | 3 |
| U | 0 | - | - | - | - | - | - |

Notes: SD, standard deviation; RSD, relative standard deviation ($100 \times (SD/\text{mean})$)

Table 15. Statistics for Olympus Vanta M-Series analyses in standard GeoChem 3-beam mode for a coarse-grained rock sample from 215 m depth in drillcore 18JBDD002

| <i>Element</i> | <i>Valid Samples</i> | <i>Mean (ppm)</i> | <i>SD (ppm)</i> | <i>RSD (%)</i> | <i>Min. (ppm)</i> | <i>Max. (ppm)</i> | <i>Range (ppm)</i> |
|----------------|----------------------|-------------------|-----------------|----------------|-------------------|-------------------|--------------------|
| Mg | 7 | 12479 | 1838 | 14.73 | 9916 | 15185 | 5269 |
| Al | 7 | 68033 | 2385 | 3.51 | 64339 | 72109 | 7770 |
| Si | 7 | 319741 | 8977 | 2.81 | 300058 | 330140 | 30082 |
| P | 7 | 2410 | 193 | 8.01 | 2091 | 2787 | 696 |
| S | 3 | 159.7 | 21.31 | 13.35 | 135 | 187 | 52 |
| K | 7 | 32168 | 1346 | 4.19 | 29786 | 33858 | 4072 |
| Ca | 7 | 12092 | 755 | 6.24 | 11378 | 13544 | 2166 |
| Ti | 7 | 8152 | 1353 | 16.60 | 6198 | 10885 | 4687 |
| V | 0 | - | - | - | - | - | - |
| Cr | 3 | 66.67 | 12.28 | 18.43 | 57 | 84 | 27 |
| Mn | 7 | 455 | 69.49 | 15.28 | 348 | 573 | 225 |
| Fe | 7 | 34944 | 1156 | 3.31 | 32873 | 36448 | 3575 |
| Co | 0 | - | - | - | - | - | - |
| Ni | 7 | 30.29 | 3.01 | 9.94 | 27 | 36 | 9 |
| Cu | 7 | 263 | 35.54 | 13.52 | 234 | 346 | 112 |
| Zn | 7 | 166 | 30.44 | 18.34 | 115 | 202 | 87 |
| As | 0 | - | - | - | - | - | - |
| Se | 0 | - | - | - | - | - | - |
| Rb | 7 | 79.43 | 3.89 | 4.89 | 73 | 85 | 12 |
| Sr | 7 | 220 | 9.15 | 4.15 | 205 | 231 | 26 |
| Y | 7 | 42.86 | 1.36 | 3.16 | 41 | 45 | 4 |
| Zr | 7 | 403 | 45.36 | 11.24 | 312 | 442 | 130 |
| Nb | 4 | 6.75 | 0.83 | 12.28 | 6 | 8 | 2 |
| Mo | 6 | 11.33 | 1.89 | 16.64 | 8 | 14 | 6 |
| Ag | 1 | 9.00 | - | - | 9 | 9 | - |
| Cd | 1 | 25.00 | - | - | 25 | 25 | - |
| Sn | 2 | 38.50 | 5.50 | 14.29 | 33 | 44 | 11 |
| Sb | 1 | 41.00 | - | - | 41 | 41 | - |
| Ba | 7 | 2274 | 93.80 | 4.13 | 2076 | 2366 | 290 |
| La | 5 | 192 | 48.98 | 25.51 | 141 | 284 | 143 |
| Ce | 7 | 299 | 56.07 | 18.74 | 220 | 389 | 169 |
| Pr | 2 | 321 | 17.50 | 5.46 | 303 | 338 | 35 |
| Nd | 2 | 663 | 32.00 | 4.83 | 631 | 695 | 64 |
| W | 0 | - | - | - | - | - | - |
| Hg | 0 | - | - | - | - | - | - |
| Pb | 7 | 32.29 | 2.12 | 6.56 | 29 | 35 | 6 |
| Bi | 0 | - | - | - | - | - | - |
| Th | 7 | 21.86 | 5.36 | 24.51 | 13 | 29 | 16 |
| U | 0 | - | - | - | - | - | - |

Notes: SD, standard deviation; RSD, relative standard deviation ($100 \times (\text{SD}/\text{mean})$)



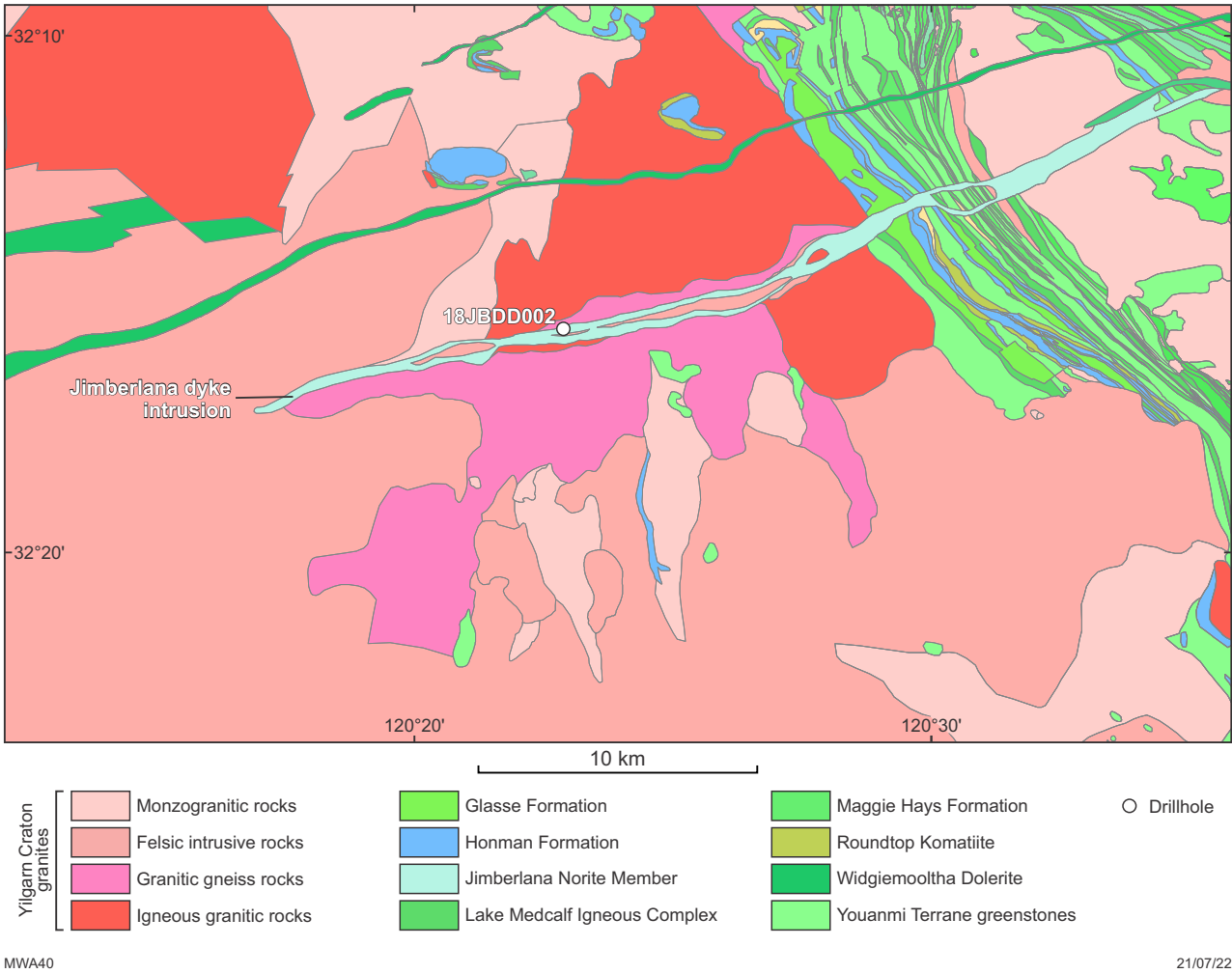


Figure 8. Regional geology and location of drillhole 18JBDD002, which intercepts the Jimberlana dyke intrusion in the Southern Cross Domain

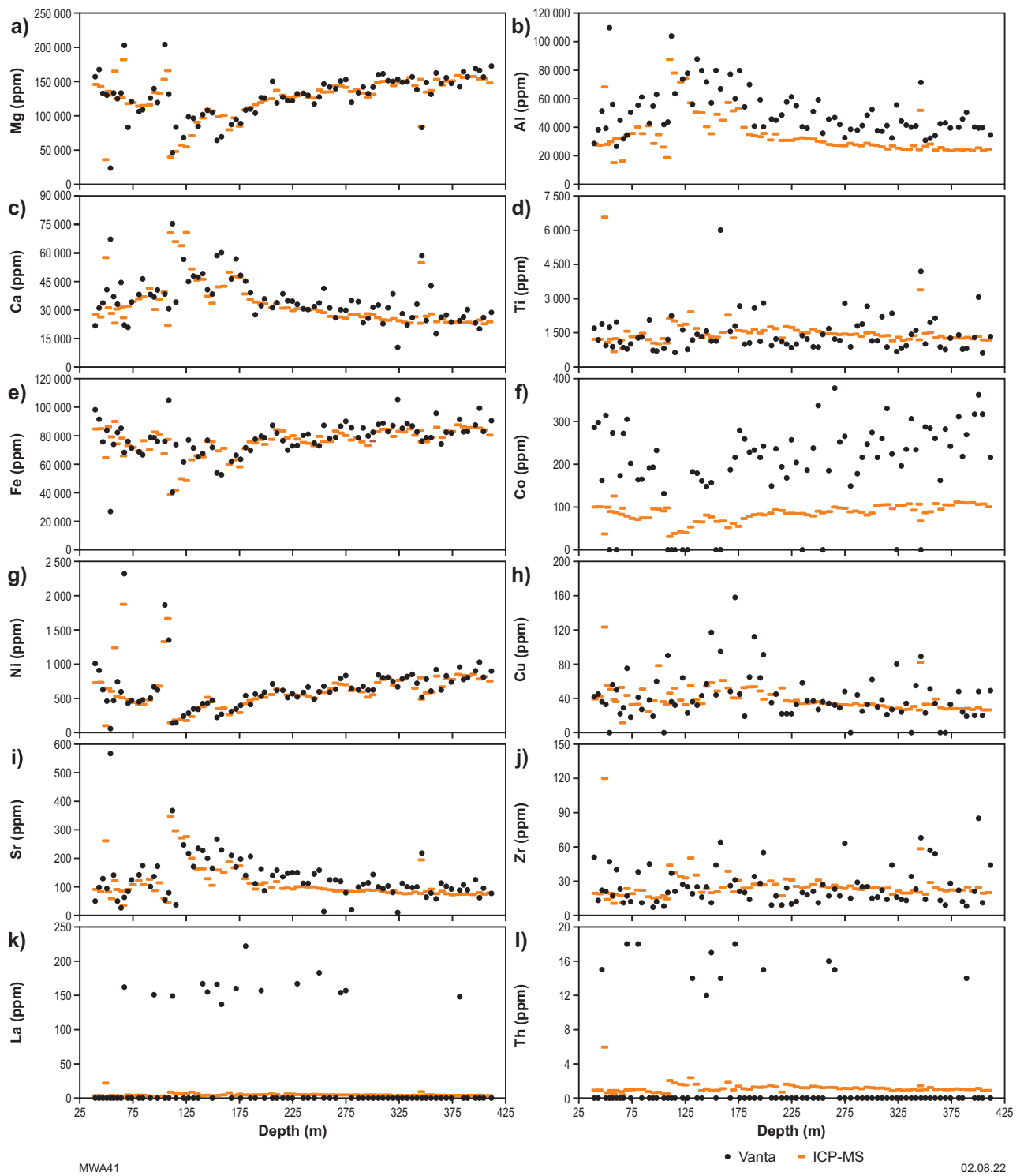


Figure 9. Comparative downhole plots of ICP-MS and Vanta M-Series pXRF assays (ppm) of drillcore 18JBDD002 for: a) Mg; b) Al; c) Ca; d) Ti; e) Fe; f) Co; g) Ni; h) Cu; i) Sr; j) Zr; k) La; l) Th

Table 16. Measured concentrations by PANalytical MagiX Fast XRF of half-core samples of Jimberlana dyke drillcore 18JBDD002

| Sample ID | GSWA 250444 | GSWA 250445 | GSWA 250446 | GSWA 250447 | GSWA 250448 | GSWA 250449 | GSWA 250450 | GSWA 250451 | GSWA 250452 | GSWA 250469 | GSWA 250453 | GSWA 250454 | GSWA 250455 | GSWA 250456 | GSWA 250458 |
|-----------|----------------|----------------|----------------|----------------|----------------|----------------|----------------|----------------|----------------|----------------|----------------|----------------|----------------|----------------|----------------|
| Depth (m) | 52.75 m | 67.45 m | 68.05 m | 68.95 m | 83.95 m | 85.25 m | 99.55 m | 103.25 m | 106.45 m | 113.95 m | 144.15 m | 166.35 m | 207.75 m | 216.05 m | 220.25 m |
| Element | (ppm) | (ppm) | (ppm) | (ppm) | (ppm) | (ppm) | (ppm) | (ppm) | (ppm) | (ppm) | (ppm) | (ppm) | (ppm) | (ppm) | (ppm) |
| Mg | 145950 | 201435 | 183946 | 125445 | 126651 | 125445 | 151981 | 176708 | 186961 | 42217 | 113383 | 103130 | 144141 | 140522 | 138110 |
| Al | 32443 | 19053 | 23605 | 41864 | 44245 | 41758 | 31173 | 28209 | 21858 | 83939 | 45357 | 56471 | 34348 | 34772 | 34772 |
| Si | 238348 | 200251 | 200766 | 248491 | 248024 | 248912 | 225446 | 200906 | 197260 | 248351 | 248257 | 248725 | 238581 | 238441 | 244611 |
| K | 1494 | 755 | 1337 | 1353 | 1586 | 1494 | 1635 | 1129 | 465 | 5321 | 2208 | 2748 | 2756 | 2241 | 3096 |
| Ca | 33305 | 19011 | 22442 | 43168 | 40595 | 40309 | 32805 | 27659 | 29589 | 71327 | 45955 | 49386 | 32805 | 32948 | 34377 |
| Ti | 1191 | 715 | 894 | 1310 | 1251 | 1310 | 1251 | 1012 | 1370 | 2978 | 1548 | 1608 | 1667 | 1548 | 1846 |
| V | 117 | 59.5 | 83 | 127 | 117 | 129 | 114 | 96. | 84 | 180 | 140 | 134 | 125 | 121 | 138 |
| Cr | 2420 | 1560 | 3340 | 2200 | 2230 | 2160 | 2550 | 3070 | 1820 | 59 | 2040 | 1800 | 2410 | 2430 | 2460 |
| Mn | 1549 | 1317 | 1471 | 1394 | 1394 | 1471 | 1471 | 1317 | 1239 | 1239 | 1394 | 1317 | 1471 | 1471 | 1471 |
| Fe | 94210 | 92889 | 110223 | 78120 | 77498 | 82317 | 100040 | 97086 | 87525 | 75788 | 83716 | 74078 | 91178 | 89624 | 87136 |
| Ni | 684 | 2090 | 1350 | 444 | 474 | 448 | 850 | 1340 | 1830 | 126 | 456 | 352 | 680 | 666 | 590 |
| Cu | 70 | 18 | 34 | 42 | 28 | 44 | 78 | 38 | 26 | 122 | 58 | 54 | 42 | 48 | 38 |
| Zn | 80 | 70 | 95 | 75 | 70 | 75 | 80 | 75 | 75 | 80 | 80 | 70 | 75 | 85 | 80 |
| Sr | 923 | 44 | 69 | 114 | 124 | 120 | 89 | 72 | 45 | 257 | 135 | 174 | 106 | 102 | 105 |
| Zr | 16 | 9 | 13 | 17 | 18 | 18 | 21 | 13 | 178 | 55 | 25 | 26 | 315 | 26 | 36 |
| Ba | 76 | 33 | 612 | 656 | 812 | 78 | 89 | 57 | 50 | 257 | 109 | 138 | 134 | 111 | 151 |

Notes: Sample depths are listed and measured at the centre of 10-cm half-core samples

Table 17. Measured concentrations by the Minalyzer CS XRF core scanner of half-core samples of Jimberlana dyke drillcore 18JBDD002

| Sample ID | GSWA 250444 | GSWA 250445 | GSWA 250446 | GSWA 250447 | GSWA 250448 | GSWA 250449 | GSWA 250450 | GSWA 250451 | GSWA 250452 | GSWA 250469 | GSWA 250453 | GSWA 250454 | GSWA 250455 | GSWA 250456 | GSWA 250458 |
|-----------|----------------|----------------|----------------|----------------|----------------|----------------|----------------|----------------|----------------|----------------|----------------|----------------|----------------|----------------|----------------|
| Depth (m) | 52.75 m | 67.45 m | 68.05 m | 68.95 m | 83.95 m | 85.25 m | 99.55 m | 103.25 m | 106.45 m | 113.95 m | 144.15 m | 166.35 m | 207.75 m | 216.05 m | 220.25 m |
| Element | (ppm) | (ppm) | (ppm) | (ppm) | (ppm) | (ppm) | (ppm) | (ppm) | (ppm) | (ppm) | (ppm) | (ppm) | (ppm) | (ppm) | (ppm) |
| Mg | 144600 | 219759 | 203312 | 122379 | 108606 | 121502 | 139395 | 183501 | 193691 | 44186 | 88441 | 79369 | 134149 | 127785 | 107907 |
| Al | 43431 | 20543 | 28414 | 63543 | 46284 | 45866 | 28979 | 30391 | 16127 | 88707 | 46102 | 56930 | 43780 | 34078 | 37997 |
| Si | 210074 | 183442 | 178980 | 218114 | 181186 | 166452 | 134546 | 145557 | 142292 | 163614 | 145452 | 150818 | 186119 | 176799 | 138598 |
| K | 1351 | 988 | 1454 | 1722 | 1400 | 1599 | 1792 | 1319 | 549 | 7696 | 2021 | 2480 | 1648 | 1079 | 1684 |
| Ca | 31463 | 18817 | 19570 | 44444 | 37420 | 34987 | 23682 | 23712 | 21860 | 69427 | 34859 | 39898 | 28038 | 26137 | 26220 |
| Ti | 978 | 590 | 715 | 1228 | 5066 | 957 | 827 | 854 | 1025 | 1619 | 1078 | 1081 | 1157 | 950 | 975 |
| V | 58 | 23.6 | 24 | 64 | 58.2 | 50 | 26 | 31 | 20.5 | 56 | 41 | 41 | 50 | 52 | 53.55 |
| Cr | 2985 | 1894 | 3276 | 2887 | 2718 | 2713 | 2112 | 3817 | 2026 | 414 | 2244 | 2192 | 2887 | 2589 | 2781 |
| Mn | 1421 | 1424 | 1382 | 1355 | 1183 | 1309 | 1280 | 1339 | 1240 | 832 | 1140 | 1105 | 1281 | 1297 | 1212 |
| Fe | 83256 | 84945 | 89712 | 68627 | 62496 | 70863 | 84606 | 82766 | 78907 | 42749 | 64086 | 59703 | 71802 | 79442 | 67750 |
| Ni | 414 | 1365 | 811 | 235 | 258 | 255 | 530 | 912 | 1389 | 108 | 233 | 191 | 343 | 379 | 311 |
| Cu | 38 | 24 | - | 39 | 23 | 21 | 26 | 48 | 27 | 48 | 45 | 44 | 20 | 41 | 35 |
| Zn | 92 | 93 | 111 | 128 | 119 | 109 | 103 | 122 | 127 | 130 | 138 | 96 | 110 | 95 | 80. |
| Sr | 90 | 33 | 75 | 127 | 153 | 139 | 83 | 62 | 35 | 321 | 153 | 176 | 103 | 90 | 133 |
| Zr | 89 | - | - | - | - | - | - | - | - | - | 105 | 110 | - | - | - |
| Ba | 259 | 90 | 112 | 227 | 231 | 374 | 380 | 242 | 380 | 822 | 449 | 447 | 155 | 185 | 426 |

Notes: Sample depths are listed and measured at the centre of 10-cm half-core samples

Table 18. Measured concentrations of half-core samples of Jimberlana dyke drillcore 18JBDD002 by Olympus Vanta M-Series pXRF

| Sample ID | GSWA 250444 | GSWA 250445 | GSWA 250446 | GSWA 250447 | GSWA 250448 | GSWA 250449 | GSWA 250450 | GSWA 250451 | GSWA 250452 | GSWA 250469 | GSWA 250453 | GSWA 250454 | GSWA 250455 | GSWA 250456 | GSWA 250458 |
|-----------|----------------|----------------|----------------|----------------|----------------|----------------|----------------|----------------|----------------|----------------|----------------|----------------|----------------|----------------|----------------|
| Depth (m) | 52.75 m | 67.45 m | 68.05 m | 68.95 m | 83.95 m | 85.25 m | 99.55 m | 103.25 m | 106.45 m | 113.95 m | 144.15 m | 166.35 m | 207.75 m | 216.05 m | 220.25 m |
| Element | (ppm) | (ppm) | (ppm) | (ppm) | (ppm) | (ppm) | (ppm) | (ppm) | (ppm) | (ppm) | (ppm) | (ppm) | (ppm) | (ppm) | (ppm) |
| Mg | 128235 | 203567 | 182624 | 113328 | 118442 | 119278 | 157858 | 197884 | 200999 | 47331 | 121106 | 89229 | 131114 | 126386 | 137400 |
| Al | 54683 | 25123 | 38480 | 67715 | 62355 | 57474 | 41256 | 36081 | 35083 | 92097 | 55983 | 81661 | 67527 | 63504 | 56301 |
| Si | 246070 | 201535 | 204686 | 254441 | 249475 | 252873 | 231743 | 223964 | 213850 | 250330 | 257281 | 257093 | 247466 | 248300 | 258660 |
| K | 1519 | 1293 | 747 | 1149 | 401 | 1361 | 1280 | 736 | 195 | 3497 | 1769 | 2985 | 728 | 579 | 813 |
| Ca | 33750 | 14767 | 23531 | 45066 | 46131 | 34676 | 28436 | 22465 | 27682 | 68926 | 39685 | 44158 | 35583 | 36875 | 34022 |
| Ti | 1040 | 822 | 525 | 1034 | 721 | 865 | 810 | 1090 | 805 | 1289 | 2029 | 2274 | 654 | 668 | 840 |
| V | 89 | - | - | 100 | 125 | 119 | 94 | - | 96 | 127 | 118 | 130 | 93 | 110 | - |
| Cr | 2109 | 1170 | 2876 | 1788 | 2071 | 1896 | 2004 | 3046 | 1420 | 77 | 1851 | 1364 | 2147 | 2262 | 2479 |
| Mn | 1448 | 1132 | 1490 | 1292 | 1261 | 1424 | 1531 | 1395 | 1189 | 1175 | 1425 | 1199 | 1359 | 1310 | 1385 |
| Fe | 81471 | 79672 | 91693 | 63941 | 67905 | 75272 | 93248 | 86555 | 83690 | 68468 | 75862 | 63904 | 74881 | 69970 | 74431 |
| Ni | 610 | 2477 | 1472 | 397 | 532 | 448 | 844 | 1344 | 2015 | 116 | 427 | 309 | 596 | 543 | 550 |
| Cu | 31 | 35 | 28 | 26 | 19 | 25 | 33 | 53 | 22 | 96 | 35 | 116 | 16 | 31 | 24 |
| Zn | 74 | 85 | 74 | 63 | 62 | 74 | 90 | 87 | 88 | 59 | 74 | 60 | 71 | 67 | 73 |
| Sr | 145 | 49 | 90 | 188 | 168 | 157 | 120 | 68 | 58 | 300 | 161 | 257 | 182 | 180 | 137 |
| Zr | 15 | 19 | 7 | 16 | 9 | 15 | 10 | 15 | 11 | 31 | 23 | 33 | 7 | 10 | 14 |
| Ba | 247 | 193 | 130 | 148 | 171 | 136 | 240 | 171 | 121 | 339 | 187 | 319 | 260 | 163 | 207 |

Notes: Sample depths are listed and measured at the centre of 10-cm half-core samples

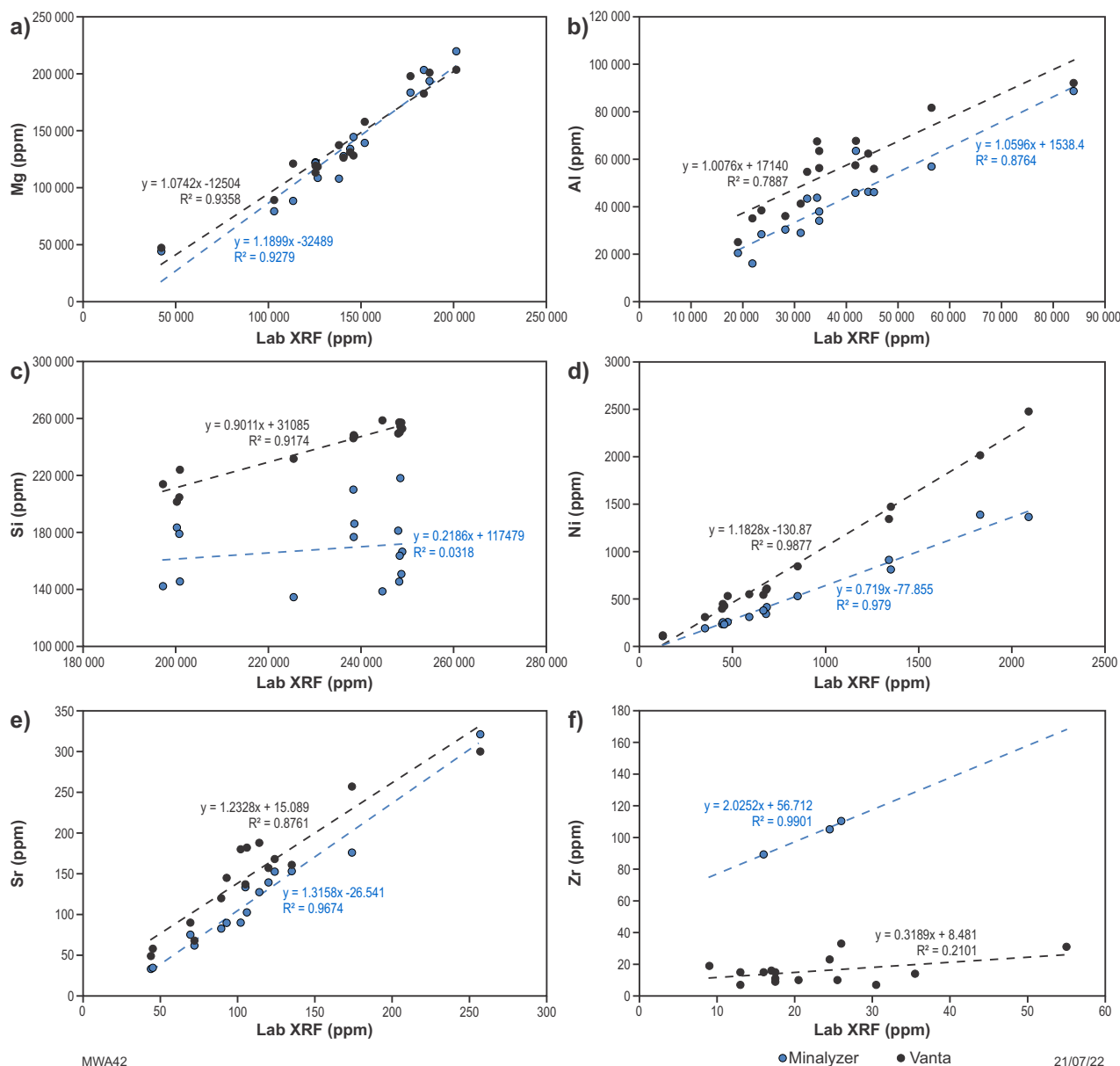


Figure 10. Comparative correlation plots of measurements (ppm) of drillcore 18JBDD002 half-core samples by Vanta M-Series pXRF (black) and Minalyzer XRF (blue) against laboratory XRF for a) Mg; b) Al; c) Si; d) Ni; e) Sr; f) Zr. Lines of best fit and statistics are computer calculated

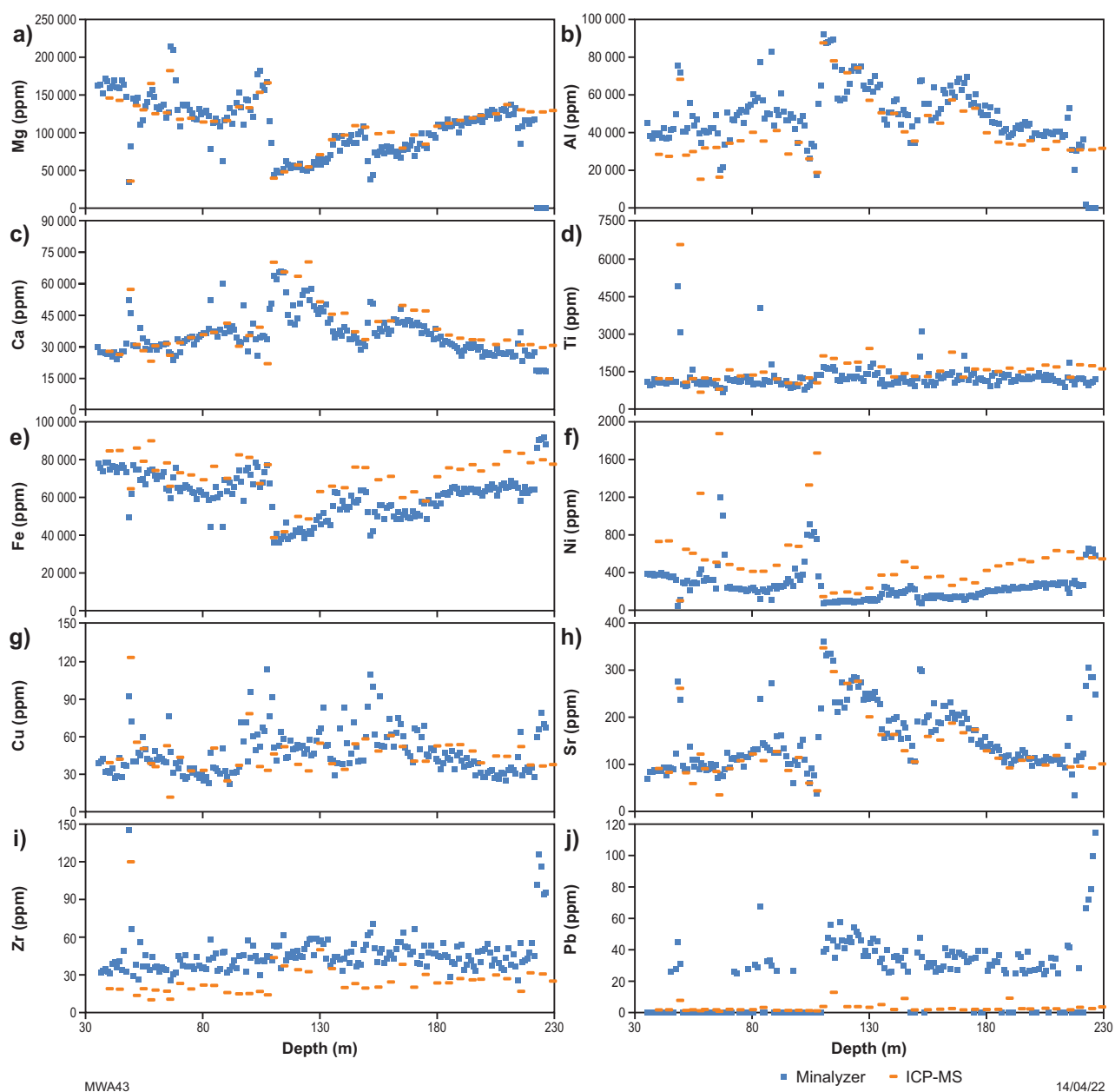


Figure 11. Comparative downhole plots of ICP-MS and Minalyzer XRF assays (ppm) of drillcore 18JBDD002 for: a) Mg; b) Al; c) Ca; d) Ti; e) Fe; f) Ni; g) Cu; h) Sr; i) Zr; j) Pb. ICP-MS values adapted from WAMEX Report A118977

This is exemplified by a sharp negative Mg feature observed at 150–153 m depth in data collected by both, the Minalyzer and Vanta, but missed by the ICP-MS assay. This corresponds to a narrow gabbroic layer within the surrounding pyroxenite, as observed by a change in mineralogy in the corresponding HyLogger scan data. Geochemical signatures of similar narrow anomalous features can be missed or lost by homogenization with surrounding rock during processing for whole-rock assaying methods (e.g. ICP-MS), if they are not visually observable by geologists and accounted for during sampling. The likelihood of missing these anomalies can be reduced by using higher-density, narrow and unbiased samples for assaying, at the expense of increasing dispersion in the results.

Partial least squares spectral modeling

It is possible to utilize the high sample density spectral data collected in the HyLogger, to create higher-resolution downhole estimates of elemental concentrations from the relatively lower-resolution pXRF data, similar to the Minalyzer assays. This can be achieved by using the partial least squares (PLS) regression modeling functionality built into The Spectral Geologist (TSG) software package used to analyse HyLogger data. Although a detailed description of PLS regression modeling is beyond the scope of this record, a simplified explanation is that linear regression algorithms are applied to model a measured variable (e.g. elemental concentration) using co-measured multispectral IR reflectance data, and the resulting PLS model applied to extrapolate data from multispectral data that lack corresponding measurements (Hecker et al., 2012). PLS modeling has previously been used to model mineralogy (Hecker et al., 2012; Stromberg et al., 2021) and petrophysical attributes (Laukamp et al., 2021) from drillcore hyperspectral IR reflectance data.

PLS modeling of downhole pXRF measurements for Mg and Zr was performed using their corresponding thermal IR spectra (TIR; 6000–14500 nm) as a training dataset. The derived models were then applied against the entire downhole TIR spectra using the inbuilt PLS scalar function, and corresponding results binned to 10 cm. The results of PLS modeling of Mg are as accurate as the ICP-MS assay results, and correlate significantly with the Minalyzer assay results (Fig. 12a,b). Although the model accurately reproduces large-scale trends, absolute correlation with Minalyzer results at the sample scale is weak, with a linear correlation (R^2) of 0.38. The correlation improves as results are binned to 1 m ($R^2 = 0.50$), suggesting that small differences in sample positions cause proportionate differences in measurements (e.g. 1 cm in 10 cm sample = 10% difference).

Near-identical downhole geochemical trends are observed between the PLS model and Minalyzer data for Zr, including narrow negative features at depths of 47–50 m, 150–153 m, and 213–216 m, narrow positive features at 57 m and 65–67 m, and a sharp boundary and general upwards trend of Mg concentration downhole from around 110 m. However, Zr concentration is overestimated by the model between 122 m and 132 m, likely due to the anomalous pXRF measurements in this region. The results for PLS modeling of Zr are less accurate than the ICP-MS assay results; however, they better capture the downhole trends compared

to the Minalyzer data (Fig. 12c,d). The model correctly identifies multiple narrow positive features, including those at depths of 48 m, 83 m, 150–153 m, and 170 m, and also better captures the elevated Zr abundance between 109 m and 138 m.

Similarly, accurate PLS models could be produced for other datasets and elements, although they will be reliant on detectable corresponding minerals or proxy features in the spectra and sufficient data to accurately train the PLS models. PLS modeling of elements with abundances below the LOQ or without strong corresponding mineral spectral features is unlikely to be modeled accurately. PLS modeling of unbiased low-resolution pXRF measurements has the potential to significantly improve geochemical assay resolutions and predict narrow geochemical anomalies that would otherwise be missed, assisting identification of areas for further sampling and analysis. This approach could significantly reduce the cost of geochemical assaying, but should be validated using more sensitive and accurate geochemical analysis methods.

Case studies

Fraser Zone Exploration Incentive Scheme drillhole 20NMDD025

Exploration core 20NMDD025 was drilled in 2020 by Independence Group NL (IGO) in the Wineye prospect in the Fraser Zone of the Albany–Fraser Orogen (Maier et al., 2016; Vocale, 2020) as a part of the Western Australian Government's Exploration Incentive Scheme to test a gravity target interpreted to potentially host a Ni-Cu deposit, similar to their nearby Nova–Bollinger Ni-Cu-Co operational deposit (Fig. 13). The drillhole mainly intercepts an amphibolite unit interpreted to be a metamorphosed norite to gabbro-norite intrusion with various minor granitic rocks and pegmatites and no significant sulfide mineralization encountered (Vocale, 2020). IGO sampled the drillcore for broad multi-elemental assays from 1-m half-core sections collected approximately every 10 m downhole, which underwent four-acid digest and fire-assay preparation techniques, and were analysed primarily by inductively coupled plasma atomic emission spectroscopy (ICP-AES).

Drillcore 20NMDD025 was selected as one of the first drillcores at GSWA to have downhole pXRF measurements routinely collected together with GSWA HyLogger hyperspectral scanning (Fig. 14a,b), due to the excellent condition of the core and the availability of quality laboratory geochemical assay results for comparison. Factory-calibrated pXRF measurements were collected using the Olympus Vanta once per tray at a constant position of 10 cm from the start of the tray, approximately one measurement per 3–4 m. Drift monitoring was performed using measurements of CRM pressed pellet NCS DC73308 every 20 shots, assay results were subsequently imported as scalars into the corresponding HyLogger dataset and manually appended to co-located spectral data. Measurements from trays 117–124, 184–206, and 231–239 were collected but subsequently lost due to data corruption issues, and have not yet been recaptured.

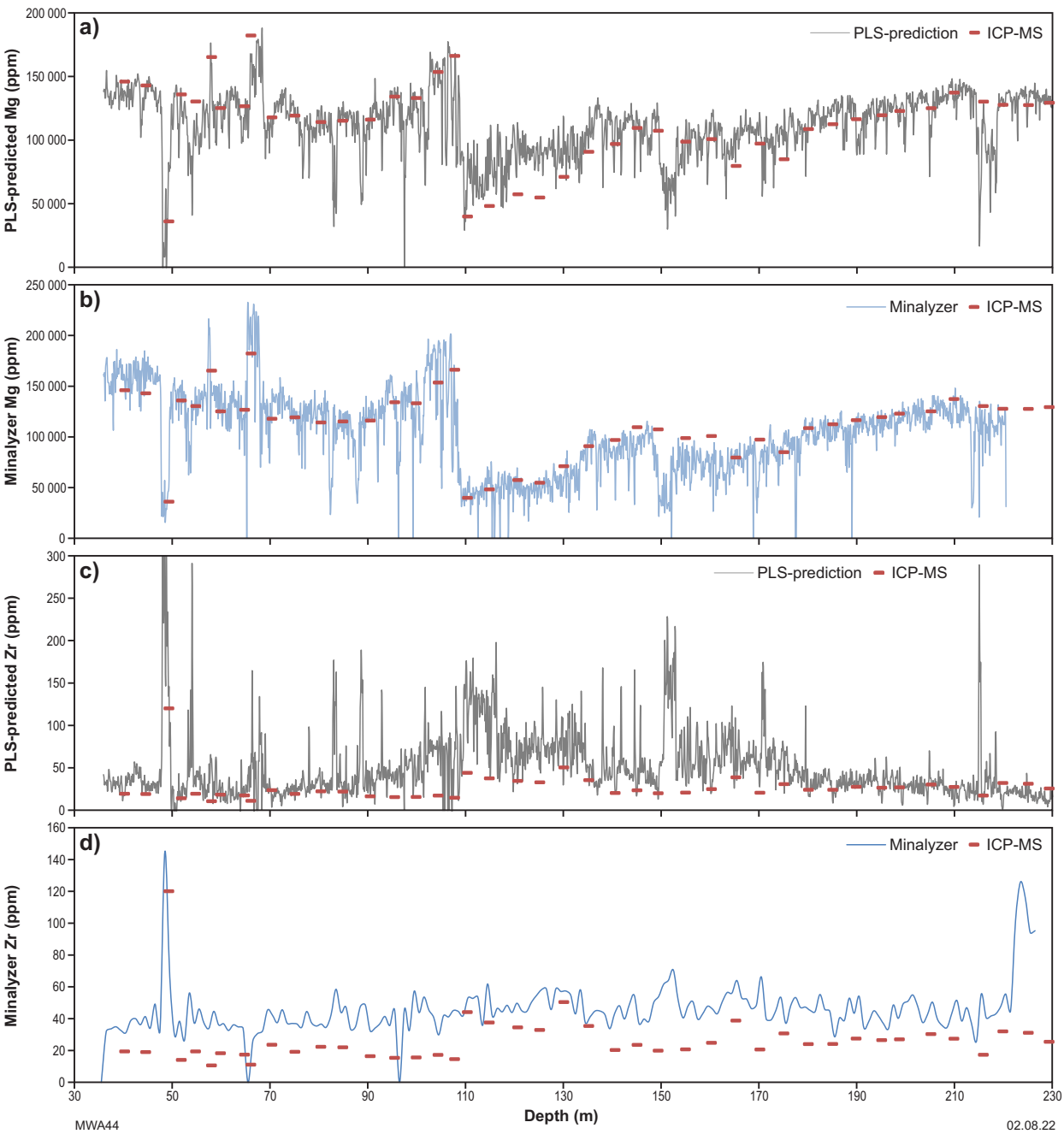
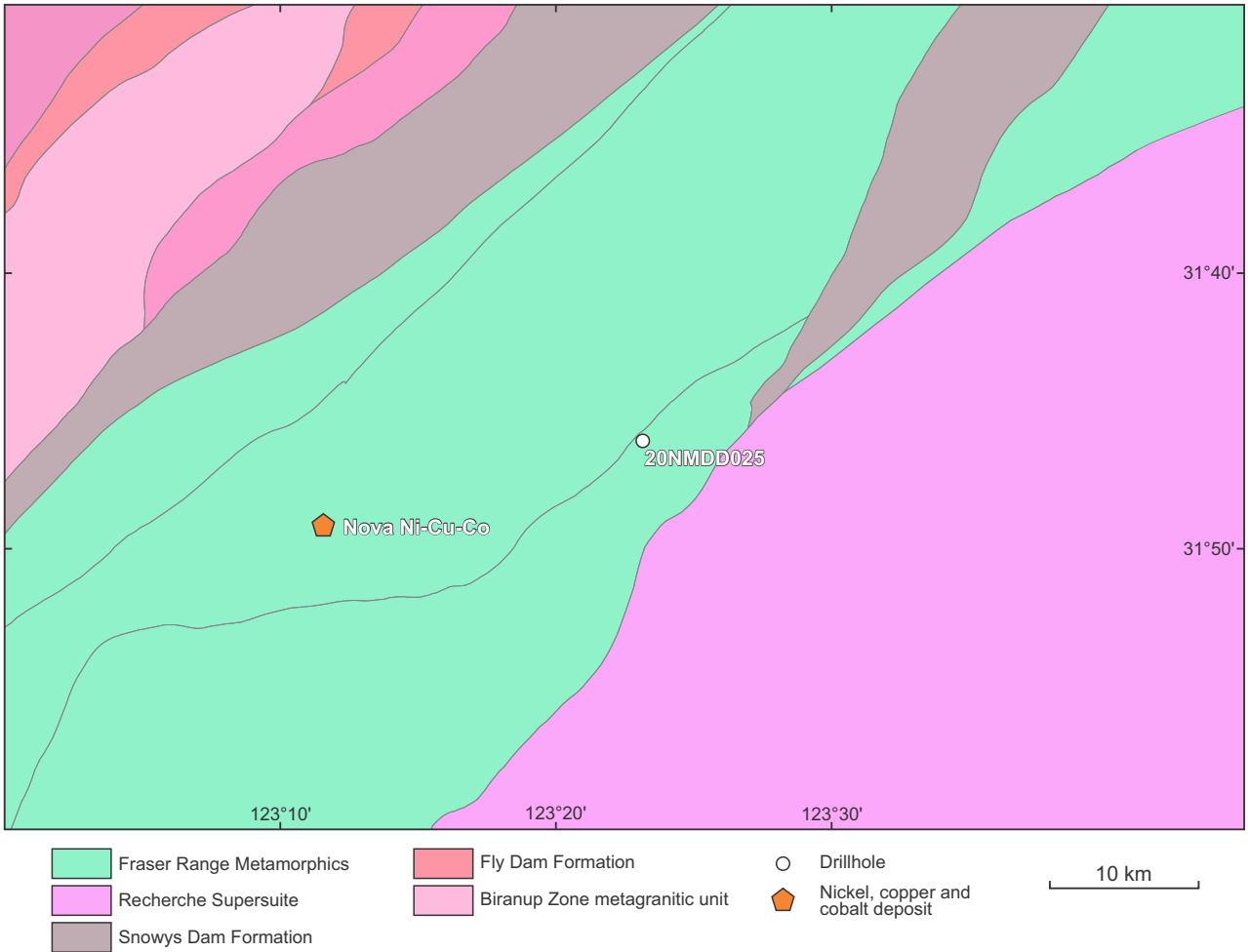


Figure 12. Comparative downhole plots of ICP-MS against: a) PLS-predicted Mg at 10-cm intervals; b) Minalyzer Mg measurements at 10-cm intervals; c) PLS-predicted Zr at 10-cm intervals; d) Minalyzer Zr measurements at 1-m intervals



MWA45

21/07/22

Figure 13. Regional geology and location of the 20NMDD025 drillhole and nearby operational Nova Ni-Cu-Co deposit in the Albany–Fraser Orogen

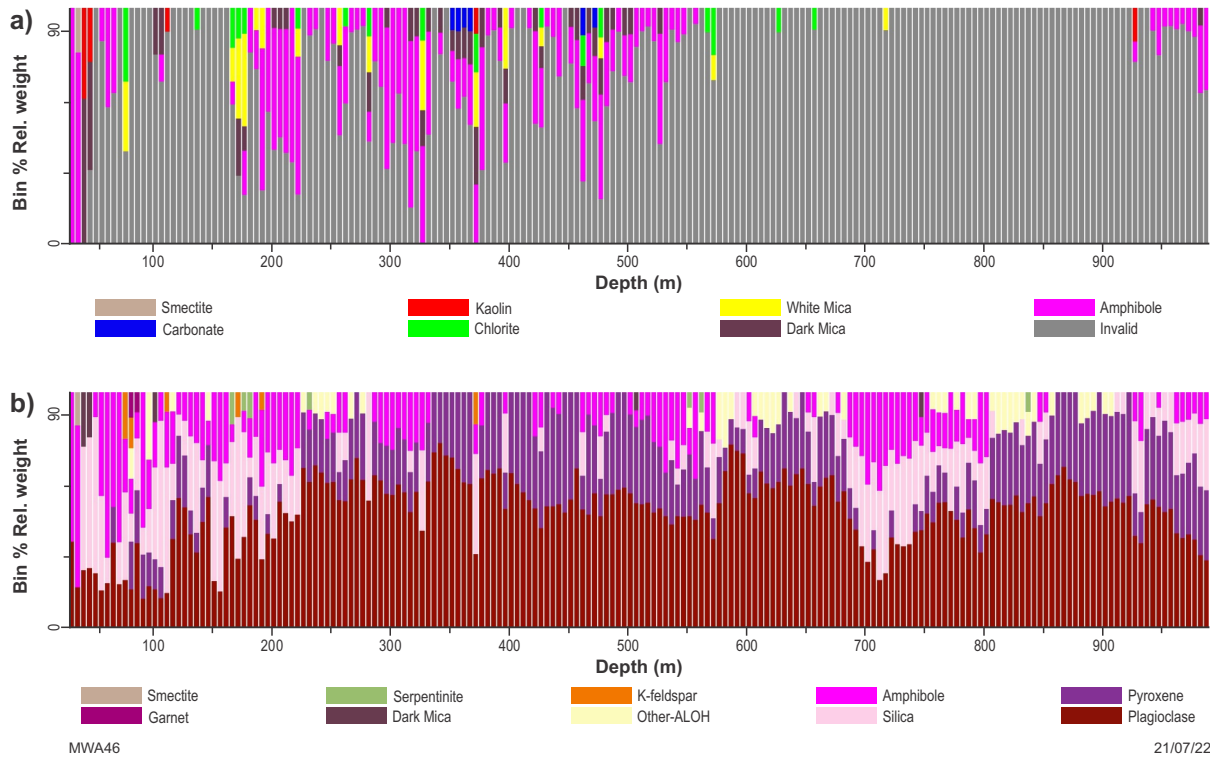


Figure 14. Simplified system-automated downhole mineral logs for 20NMDD025 drillcore from HyLogger: a) shortwave infrared (SWIR); b) thermal infrared (TIR) scan data

Comparative downhole plots of pXRF and ICP-AES assay data show good correlation for elements above the LOQ (Figs 15a–r). The larger homogenized samples used for ICP-AES analysis show less dispersion than single-shot pXRF measurements, although pXRF assay results accurately reproduce geochemical trends and concentrations for both, major (e.g. Mg, Ti) and trace (e.g. Ni, Y) elements. Two distinct magmatic units or phases can be identified, an upper phase (high Mg, low Fe, Ti, and Y) from about 110–550 m depth and a lower phase (low Mg, high Fe, Ti, and Y) below 550 m depth. The upper phase has a more primitive signature with higher Ni and Cr concentrations and an elevated Mg number and Cr/V ratio (Winter, 2010) consistent between the ICP-AES and pXRF assays (Figs 15s,t). Yttrium concentration peaks around 700 m and likely represents high concentrations of amphiboles and apatite (Winter, 2010).

Elevated P concentrations >5000 ppm are observed in pXRF measurements at 66–108 m, 528–680 m, and 789–877 m. Similarly, elevated P concentrations are observed in ICP-AES assay results, although elevated concentrations in the lowermost region are more spatially limited to 865–875 m depth compared to the Vanta results. Elevated P in these sections is consistent with corresponding high concentrations of apatite, likely the predominant P-bearing phase, in automated HyLogger spectral interpretations (Figs 16a,b). Hence, pXRF measurements have the potential to validate the interpreted presence of apatite in drillhole 20NMDD025 from spectral reflectance data. Relatively low apatite abundance interpreted at 789–850 m that is not consistent with elevated P concentrations in Vanta measurements may reflect the analysis of large apatite grains by pXRF in this interval or the presence of another P-bearing phase. Additional validation, including X-ray diffraction analysis, may be required to clarify the anomaly in this interval and serve as an example of pXRF assays guiding sampling.

Southern Carnarvon Basin GSWA Barrabiddy 1 well

GSWA Barrabiddy 1 is a stratigraphic well drilled by GSWA in 1996, on the Wandagee Ridge of the Gascoyne Platform in the Southern Carnarvon Basin (Fig. 17), primarily aimed at testing the source-rock potential of the Devonian Gneudna Formation (Mory and Yasin, 1999). GSWA Barrabiddy 1 was drilled through the Cretaceous Winning Group succession, including the Gearle Siltstone (to 96 m), Windalia Radiolarite (96–145 m), Windalia Sandstone Member (145–172 m), Muderong Shale (172–191 m), and through an unconformity into the Devonian Munabia Formation (below 191 m), before terminating at 238 m due to drilling difficulties and sidetracked by GSWA Barrabiddy 1A (Mory and Yasin, 1999). Subsequently, Rio Tinto sampled the core chips in 1999 for a multi-elemental chemical assay, to investigate the potential for carbonate-hosted base metal mineralization (Broadbent, 2000).

The chips were collected by Rio Tinto at 25-cm intervals and collated into 2–5 m bins, before being prepared by crushing and four-acid digest, and analysed by a combination of ICP-AES (P, V, Cr, Mn, Fe, Ni, Cu, and Zn) and ICP-MS (As, Sr, Mo, Ag, Cd, Sb, Ba, W, Pb, Bi, Th, and U). The existence of consistent and accurate multi-elemental downhole assays

for GSWA Barrabiddy 1, which typically do not exist for petroleum and historical mineral cores, provided a suitable dataset to compare with downhole pXRF assays collected alongside HyLogger spectral scanning data (Fig. 18a,b). Factory-calibrated pXRF measurements were collected using the Olympus Vanta once per tray at a constant position of 10 cm from the start of the tray, approximately one measurement per 5–6 m. Drift monitoring was performed using measurements of CRM pressed pellet NCS DC73308 every 20 shots, and assay results were subsequently imported as scalars into the corresponding HyLogger dataset and manually appended to co-located spectral measurements.

Comparative downhole plots of pXRF and ICP-AES/ICP-MS assay data show good correlation and accuracy for elements above the LOQ (Fig. 19a–j). Measurements of Mo and Th measurements by pXRF replicate downhole geochemical trends from the laboratory assays (Fig. 19k,l); however, they are overestimated and show greater dispersion, likely due to concentrations of these elements approaching the LOQ. Similarly, P weakly correlates and is significantly dispersed compared to the laboratory assay (Fig. 19a), although the low concentration of this element suggests only trace P-bearing minerals are present, which may easily be missed by spot pXRF measurements. Anomalous Ba concentrations at 58.75 m and 59.1 m in the laboratory assays represent baryte nodules, which were missed by the broader pXRF assay. Of the elements above the LOQ not represented in the laboratory assays, only Si and S show significant dispersion and indiscernible trends in pXRF assays (Fig. 19n,o), with other elements revealing clear downhole trends (Fig. 19m,p–t).

Abrupt geochemical changes are observed at the boundaries between the Gearle Sandstone, Windalia Radiolarite, and Windalia Sandstone in pXRF assays for Al, K, Ti, Fe, Ni, Cu, Sr, Zr, and Pb, which correspond to changes in mineralogy observable in the HyLogger scan data. The Windalia Sandstone is distinguished by a distinct elevated Mn peak and Muderong Shale by an elevated Zn peak, with an elevated Zr and Ba peak observed across both units. The Munabia Formation is best distinguished by elevated K and Ba concentrations, but is otherwise poorly discernible by geochemical trends measurable with the default Vanta analytical suite, despite clear changes in spectral mineralogy as measured by the HyLogger instrument. Only simple single-element trends have been considered thus far and it is possible that element ratios may prove to be a better tool to distinguish the boundaries between the various sedimentary units.

The apparent success in using broad single-shot pXRF assays to replicate laboratory assays and discern lithological boundaries for sedimentary sequences demonstrates the value of collecting downhole geochemical assays from petroleum and historical mineral cores. Inorganic geochemical fingerprinting of sedimentary sequences by pXRF measurement of cores can be applied to lithological classification of petroleum ditch cuttings and chips, to distinguish obscure boundaries in drillcore, and assess potential prospectivity. Observations from this well could be applied to measurements collected from nearby wells (e.g. Wandagee Corehole 1) to test this concept, and potential for this technique to be used for well correlation, although this is beyond the scope of this report.

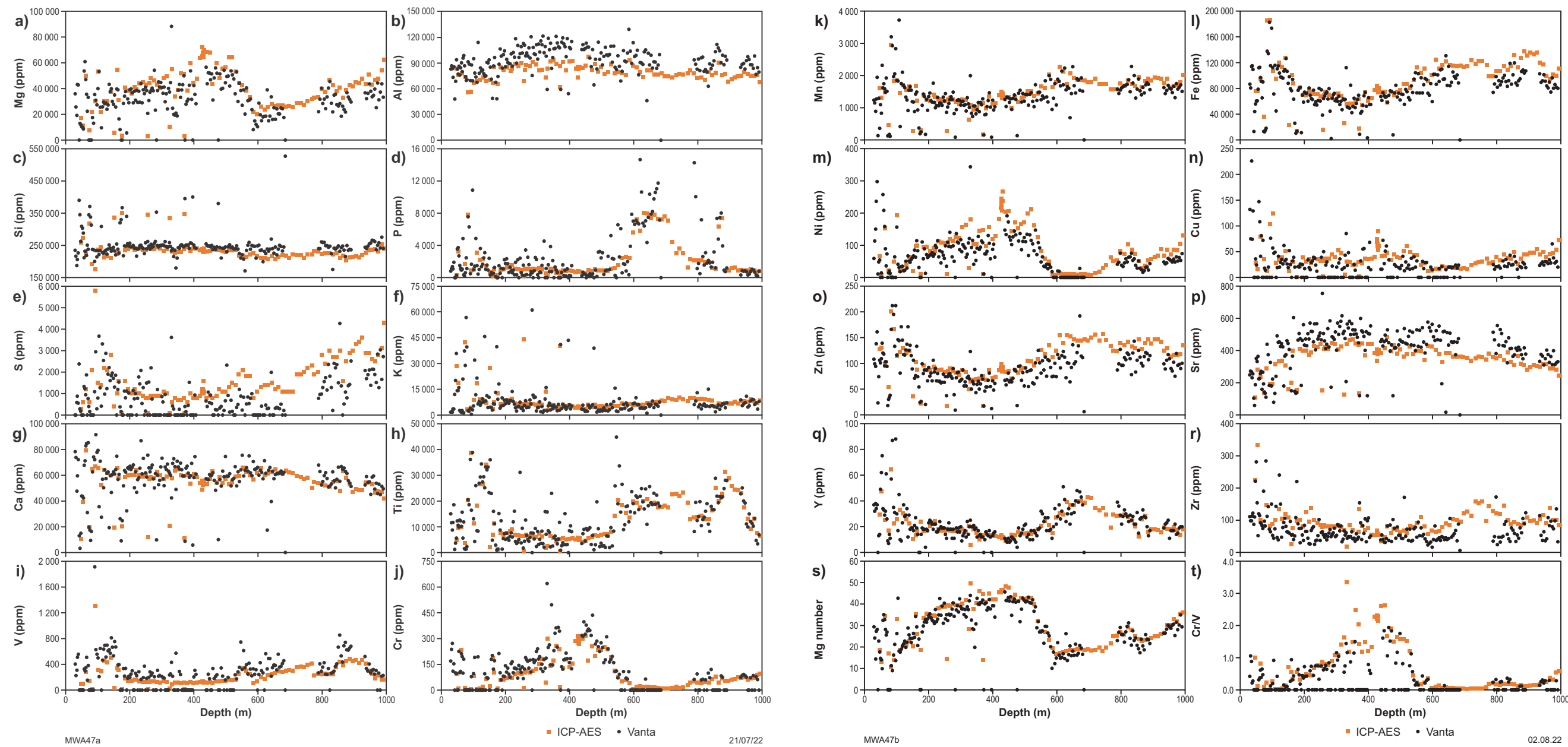


Figure 15. Comparative downhole plots of ICP-AES and Vanta M-Series pXRF assays (ppm) of drillcore 20NMDD025 for: a) Mg; b) Al; c) Si; d) P; e) S; f) K; g) Ca; h) Ti; i) V; j) Cr; k) Mn; l) Fe; m) Ni; n) Cu; o) Zn; p) Sr; q) Y; r) Zr; s) calculated Mg number; t) calculated Cr/V ratio. ICP-AES values adapted from WAMEX Report A124819

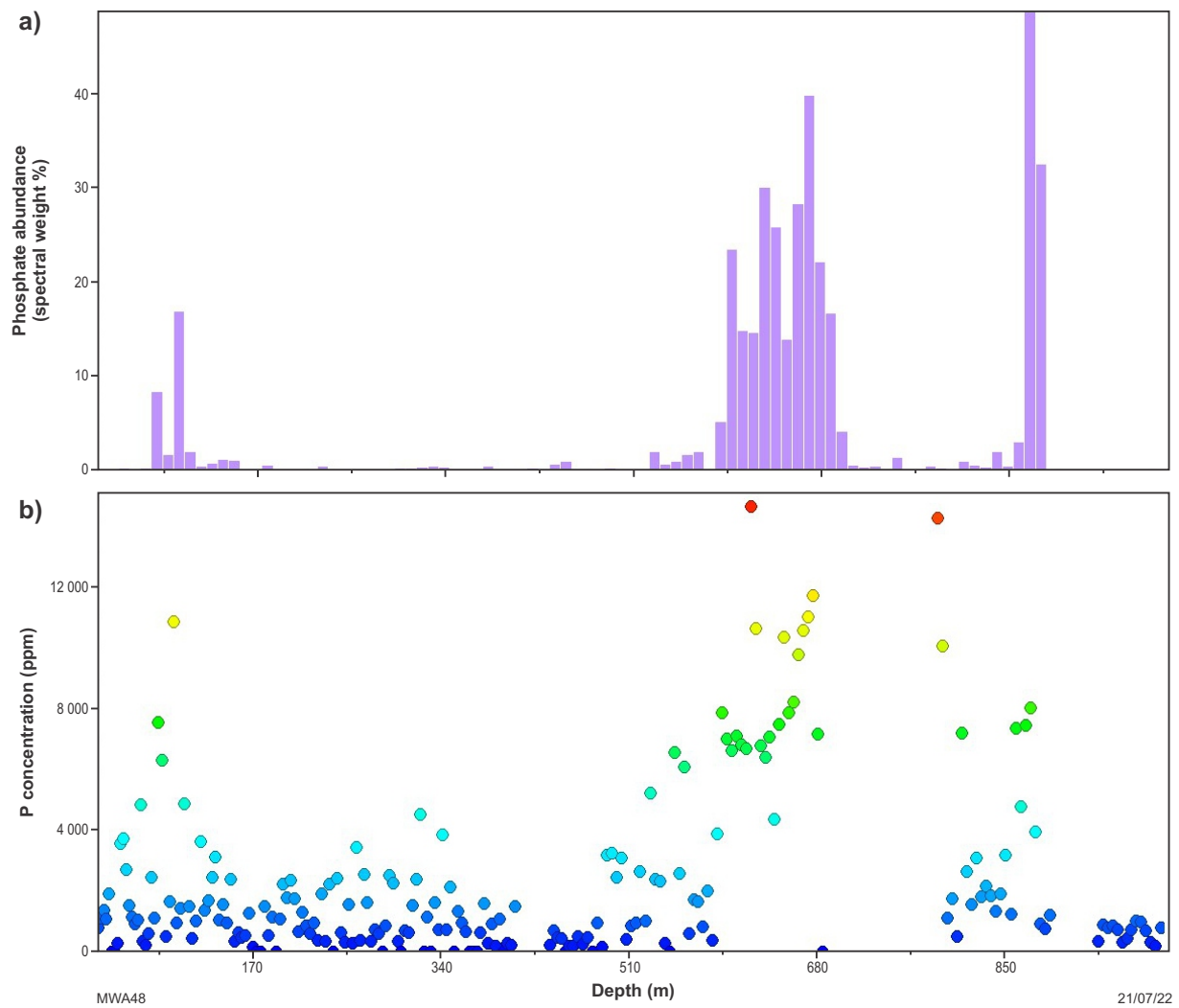
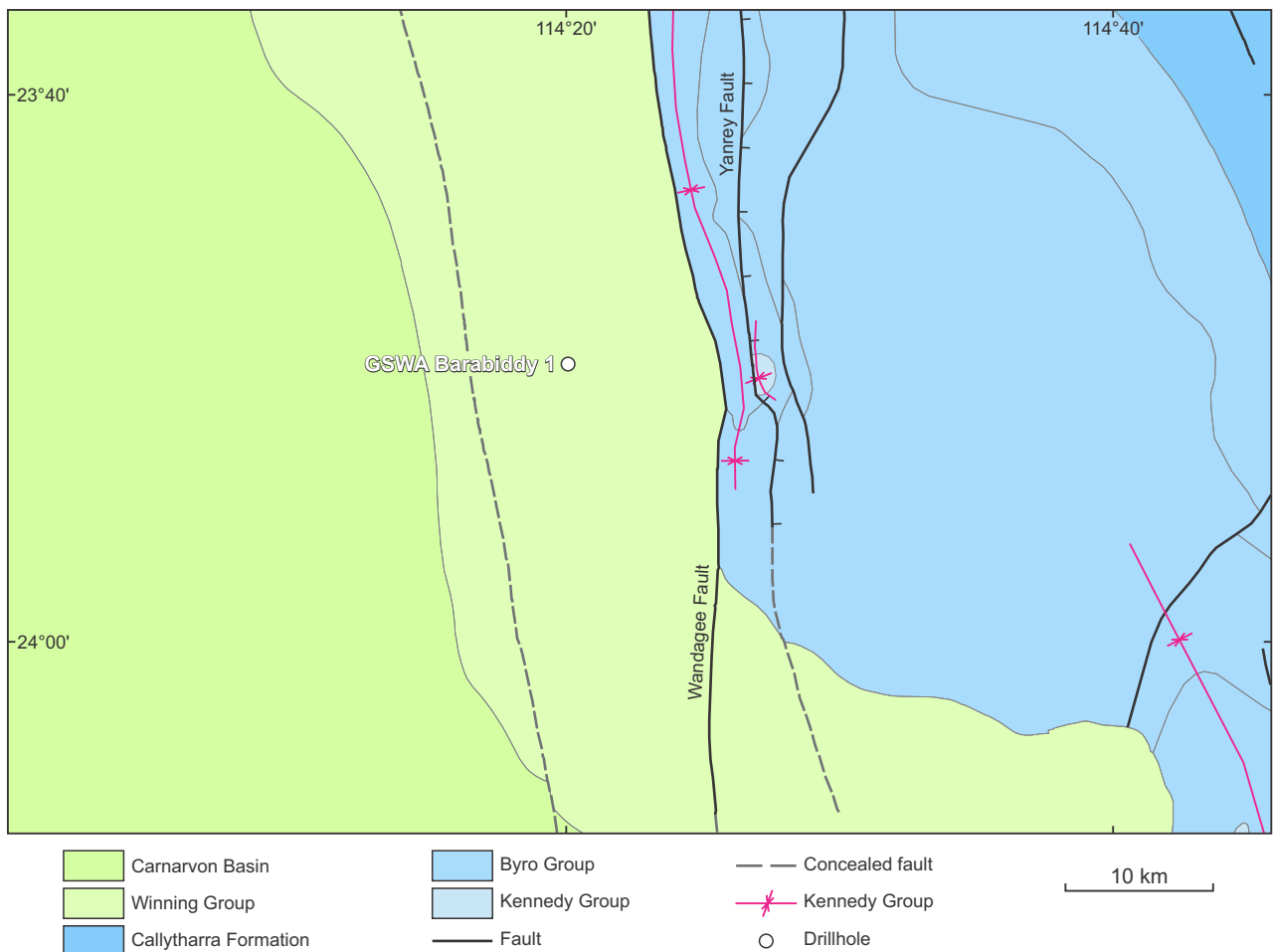


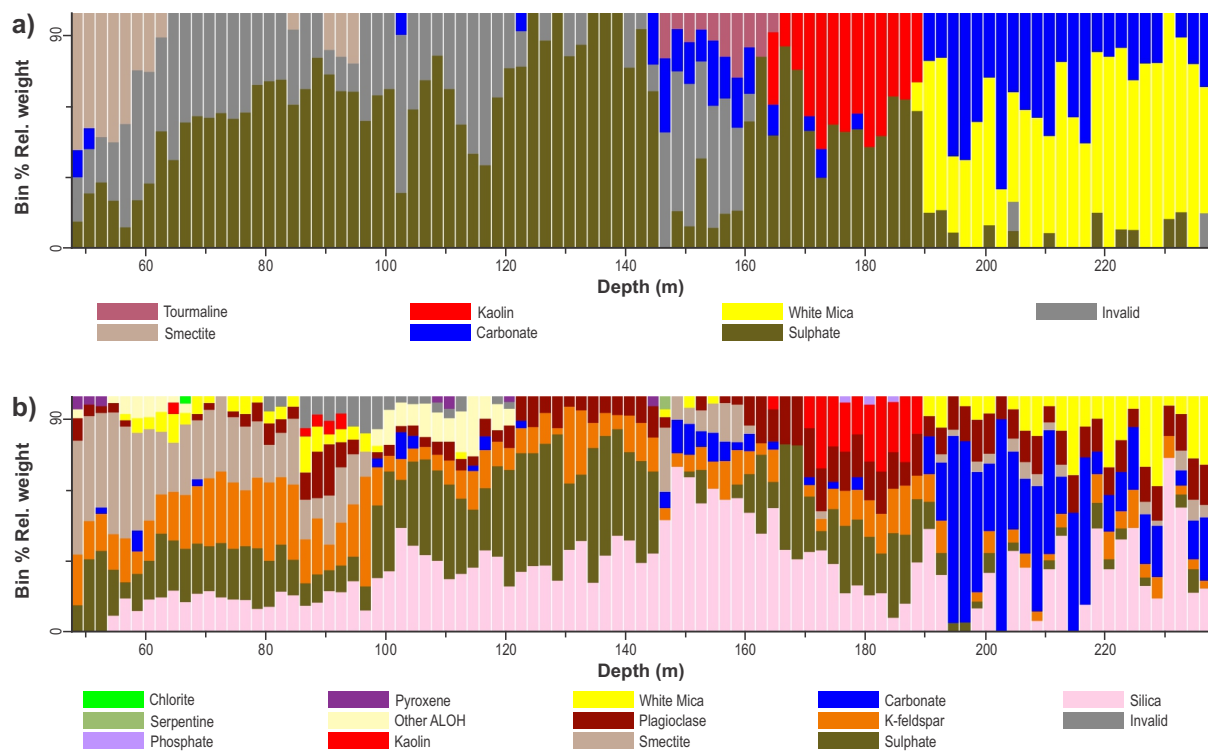
Figure 16. Comparative plots of downhole: a) system-automated phosphate mineral abundance measurements from HyLogger TIR scan data; b) Vanta M-Series pXRF measured P concentration, demonstrating the correlation between P content and P-bearing mineral abundance



MWA49

21/07/22

Figure 17. Regional geology and location of the GSWA Barrabiddy 1 in the Southern Carnarvon Basin



MWA50

21/07/22

Figure 18. Simplified system-automated downhole mineral logs for the GSWA Barrabiddy 1 drillcore from HyLogger: a) shortwave infrared (SWIR); b) thermal infrared (TIR) scan data

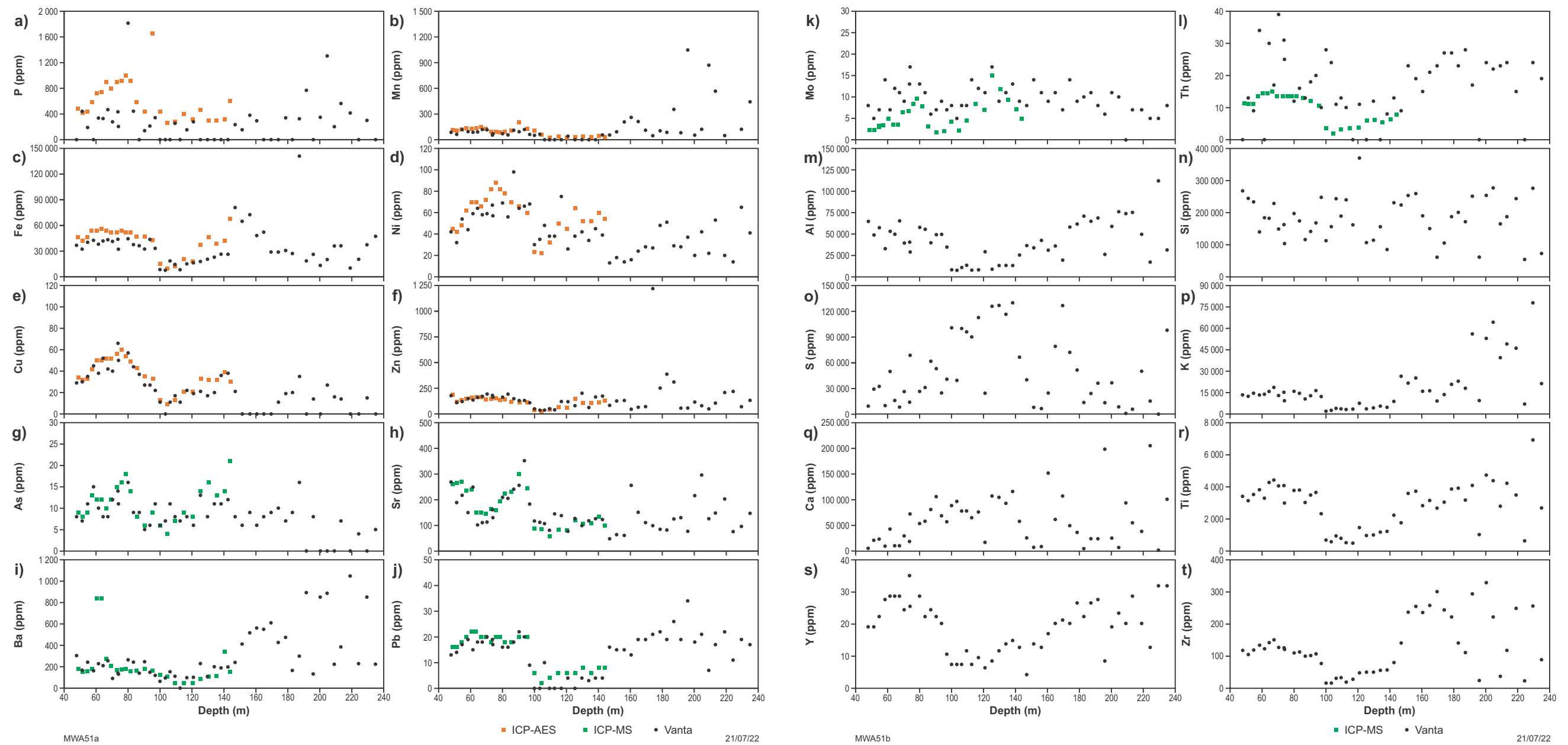


Figure 19. Comparative downhole plots of Vanta M-Series pXRF assays (ppm) of drillcore GSWA Barrabiddy 1 against ICP-AES assays for: a) P; b) Mn; c) Fe; d) Ni; e) Cu; f) Zn; and against ICP-MS assays for g) As; h) Sr; i) Ba; j) Pb; k) Mo; l) Th. Downhole plots of Vanta M-Series pXRF assays (ppm) only of drillcore GSWA Barrabiddy 1 for: m) Al; n) Si; o) S; p) K; q) Ca; r) Ti; s) Y; t) Zr. ICP-MS/ICP-AES values (ppm) adapted from Broadbent (2000)

Core library services

Access to downhole portable XRF data

Downhole pXRF assays are now routinely collected for many of the drillcores scanned with the GSWA HyLogger 3-2 since July 2020. Drift monitoring is performed by GSWA by analysis of silica blanks and powdered standard NCS DC73308 every 20 shots, and data are calibrated using factory settings to enable user calibrations with external standards. The factory-calibrated data are imported as scalars into the corresponding HyLogger datasets and manually appended to co-located spectral measurements, enabling direct comparison of geochemistry and spectrally derived mineralogy.

Collected pXRF assay data will also be made available as CSV files for download alongside GSWA HyLogger TSG datasets through the DMIRS GeoVIEW.WA online mapping portal (dmirs.wa.gov.au/geoview) as data is processed. Details of drillholes with associated pXRF data will be provided through the GSWA HyLogger scanning list available on the DMIRS HyLogger webpage (dmirs.wa.gov.au/HyLogger), which provides metadata and links to HyLogger data (e.g. tray images, TSG datasets, summary reports) for drillcores scanned by GSWA.

Requests for portable XRF analysis

GSWA currently offers a complimentary service analysing core and chip samples from the Perth Core Library collections, using the Olympus Vanta pXRF instrument. External users can email requests for pXRF analysis (corelibrary.requests@dmirs.wa.gov.au) once viewing of the relevant material has been approved. Requests for complimentary pXRF data are currently limited to 50 analyses per viewing request and are performed by trained department personnel. The generated data is delivered as CSV files and released to open files as soon as practicable, although short periods of confidentiality may be negotiated. External CRM and project-based SRM may also be analysed upon approval, for purposes of calibration.

Requests for benchtop XRD analysis

A similar service is also offered for mineral analysis using the GSWA benchtop X-ray diffractometer (pXRD; Wawryk and Hancock, 2019) for samples from the Perth and Kalgoorlie core libraries. Analysis by pXRD is currently limited to one sample per viewing request, performed by trained department personnel and interpreted by GSWA geologists. Generated data is released as open files, and delivered as raw data files and a table of interpreted mineralogy.

lithologies, as pathfinders to mineralization, measurement of alteration and weathering intensity, characterization of metamorphic history, and provenance of igneous rocks (Morris, 2009; Winter, 2010). Although less commonly utilized by sedimentary and petroleum geologists, ratios of major and trace elements have previously been used as proxies to determine various facies and other parameters of sedimentary sequences, including provenance, weathering intensity, paleoredox conditions, paleoclimatic conditions, and paleosalinity (Han et al., 2020; Sajid et al., 2020).

Continued developments in pXRF technology have resulted in increasingly quick, precise and accurate instruments with improved elemental suites and detection limits. Testing of the Olympus Vanta M-Series pXRF instrument obtained by the GSWA demonstrates superior analytical results compared to data from preceding Thermo Fisher Niton XL3t GOLDD+ pXRF instruments, with improved LOD and precision, while requiring about one-third of the analytical time. Downhole geochemical assays collected using the Olympus Vanta are also found to be accurate and replicate trends from more sensitive laboratory techniques, including laboratory XRF, and ICP-MS and ICP-AES whole-rock analysis. However, this is achieved with minimal sampling volumes and sample preparation, and results are returned almost instantaneously. In addition, pXRF is a non-destructive technique, allowing data to be collected repeatedly, maximizing remaining sample volumes for other analytical techniques.

Excellent geochemical trends can be captured, and anomalies identified with a regular, unbiased but non-intensive workflow as presented here with the Olympus Vanta instrument. Collection of co-located pXRF measurements alongside hyperspectral scanning at the resolution of a single shot at a regular location once per core tray is sufficient to reproduce data captured by larger whole-core laboratory assays, while reducing operational downtime and data processing complexity for the HyLogger. Co-located spectral and geochemical data are useful for validating and mapping complex mineralogy and the application of advanced modeling techniques to high-resolution spectral data has the potential to transform low-resolution pXRF assays into high-resolution downhole models of chemistry akin to Minalyzer datasets, further adding to the utility of this technique and workflow. The low cost and simple operation make this technique an excellent tool to gather reconnaissance geochemical data and guide further sampling, reducing sampling costs, resources, and personnel time.

Conclusions

The utility of downhole geochemical assaying has been long recognized by geologists, and is routinely utilized by the minerals industry (Morris, 2009; Winter, 2010; Lemi re and Harmon, 2021). Trends and anomalies in bulk and trace elements, and their ratios can be used for a variety of purposes, including classification and identification of

References

- AusQuest Limited 2019, Jimberlana West project, diamond drilling core assay data: Geological Survey of Western Australia, Statutory Mineral Exploration Report A118977, <www.dmir.s.wa.gov.au/wamex>.
- Broadbent, G 2000, Exploration Report No. 24806: Rio Tinto Exploration Pty Ltd: Geological Survey of Western Australia, Statutory petroleum exploration report G31432A1, 11p.
- Brouwer, P 2010, Theory of XRF: Getting acquainted with the principles (3rd edition): PANalytical B. V., Almelo, Netherlands, 62p.
- Fluxana 2015, Fluxana Reference Materials for Minerals: FXMM-0015-05, Bedburg-Hau, Germany, 156p., viewed 24 May 2021, <www.spectroaps.sk/wp-content/uploads/Fluxanacatalog_minerals_web_2015.pdf>.
- Gallhofer, D and Lottermoser, BG 2018, The influence of spectral interferences on critical element determination with portable X-ray fluorescence (pXRF): Minerals, v. 8, no. 8, doi:10.3390/min8080320.
- Han, S, Zhang, Y, Huang, J, Rui, Y and Tang, Z 2020, Elemental geochemical characterization of sedimentary conditions and organic matter enrichment for lower Cambrian shale formations in Northern Guizhou, South China: Minerals, v. 10, no. 9, doi:10.3390/min10090793.
- Hancock, EA, Green, AA, Huntington, JF, Schodlok, MC and Whitbourn, LB 2013, HyLogger-3: implications of adding thermal-infrared sensing: Geological Survey of Western Australia, Perth, Western Australia, Record 2013/3, 24p.
- Hancock, EA and Huntington, JF 2010, The GSWA HyLogger: Rapid spectral analysis and its application in detecting mineralization, in GSWA extended abstracts: promoting the prospectivity of Western Australia: Geological Survey of Western Australia, Record, p. 10–13.
- Hecker, C, Dilles, JH, van de Meijde, M and van der Meer, FD 2012, Thermal infrared spectroscopy and partial least squares regression to determine mineral modes of granitoid rocks: Geochemistry Geophysics Geosystems G3, v. 13, no. 3, doi:10.1029/2011GC004004.
- Kawai, J, Yamasaki, K and Tanaka, R 2019, Fundamental parameter method in X-ray fluorescence analysis: Encyclopedia of Analytical Chemistry: Applications, Theory and Instrumentation, doi:10.1002/9780470027318.a9666.
- Klein, C and Dutrow, B 2007, Manual of Mineral Science (23rd edition): Wiley, Hoboken, US, 675p.
- Laukamp, C, Francis, N, Hauser, J, Gopapkrishnan, S and Mule, S 2021, Modelling of petrophysical from hyperspectral drill core data collected from the Osborne Cu–Au deposit, Mount Isa Inlier, Queensland, in Abstract Volume Number #133 edited by Geological Society of Australia: Australian Earth Sciences Convention 2021: Core to Cosmos, Hobart, Tasmania, 9–12 February 2021: Geological Society of Australia, p. 45.
- Lemière, B and Harmon, RS 2021, XRF and LIBS for field geology, in Portable spectroscopy and spectrometry: Volume II: Applications edited by RA Crocombe, PE Leary, BW Kammrath and HC Lee: Wiley, Hoboken, New Jersey, USA 2, p. 455–498.
- Maier, WD, Smithies, RH, Spaggiari, CV, Barnes, S-J, Kirkland, CL, Kiddie, O and Roberts, MP 2016, The evolution of mafic and ultramafic rocks of the Mesoproterozoic Fraser Zone, Albany–Fraser Orogen, and implications for Ni-Cu sulfide potential of the region: Geological Survey of Western Australia, Record 2016/8, 49p.
- Morris, PA 2007, Composition of the Bunbury Basalt (BB1) and Kerba Monzogranite (KG1) geochemical reference materials, and assessing the contamination effects of mill heads: Geological Survey of Western Australia, Record 2007/14, 22p.
- Morris, PA 2009, Field-portable X-ray fluorescence analysis and its application in GSWA: Geological Survey of Western Australia, Record 2009/7, 23p.
- Mory, AJ and Yasin, AR 1999, GSWA Barrabiddy 1 and 1A well completion report, Wandagee Ridge, Southern Carnarvon Basin, Western Australia: Geological Survey of Western Australia, Record 1999/3, 84p.
- Olympus 2016, Axon Technology: A revolution in X-ray fluorescence: Olympus Corporation of the Americas, Waltham, US, 1p., viewed 23 August 2021, <www.olympus-ims.com/en/service-and-support/downloads/>.
- Olympus 2018, Vanta VMR Geochemistry LOD: 920-432-EN Rev. B: Olympus Corporation of the Americas, Waltham, US, 1p., viewed 18/11/21.
- Olympus 2019, Vanta Specifications: 920-404-EN Rev. H: Olympus Corporation of the Americas, Waltham, US, 2p., viewed 28 August 2021, <www.olympus-ims.com/en/downloads/download/?file=285217494&fl=en_US&inline>.
- Olympus 2020, X-ray fluorescence: Cutting out the noise, Waltham, US, 14p., viewed 23 November 2021, <www.olympus-ims.com/en/service-and-support/downloads/>.
- Olympus 2021, Vanta Family X-Ray Fluorescence Analyzer User's Manual: DMTA-10072-01EN: Olympus Scientific Solutions Americas, Waltham, MA, 154p., viewed 23 August 2021, <www.olympus-ims.com/en/service-and-support/downloads/>.
- Piorek, S 2021, Handheld X-Ray fluorescence (HHXRF), in Portable spectroscopy and spectrometry: Volume II: Applications edited by RA Crocombe, PE Leary, BW Kammrath and HC Lee: Wiley, Hoboken, New Jersey, USA 2, p. 423–454.
- Rousseau, RM 2002, Correction for long-term instrumental drift: X-Ray Spectrometry, v. 31, no. 6, p. 401–407, doi:10.1002/xrs.582.
- Rousseau, RM 2013, How to apply the fundamental parameters method to the quantitative X-ray fluorescence analysis of geological materials: Journal of Geosciences and Geomatics, v. 1, no. 1, p. 1–7, doi:10.12691/jgg-1-1-1.
- Rudnick, RL and Gao, S 2014, Composition of the continental crust, in Treatise on geochemistry edited by HD Holland and KK Turekian: Elsevier, Oxford, UK, vol. 4.1, p. 1–51.
- Sajid, Z, Ismail, MS, Zakariah, MNA, Tsegab, H, Vintaned, JAG, Hanif, T and Ahmed, N 2020, Impact of paleosalinity, paleoredox, paleoproductivity/preservation on the organic matter enrichment in black shales from Triassic turbidites of Semanggol Basin, Peninsular Malaysia: Minerals, v. 10, no. 10, doi:10.3390/min10100915.
- Stromberg, J, Schlegel, T, Pejic, B, Birchall, R and Shelton, T 2021, Deriving quantitative alteration mineralogy from TIR Hyperspectral data in IOCG Systems, in Abstract Volume Number #133 edited by Geological Society of Australia: Australian Earth Sciences Convention 2021: Core to Cosmos, Hobart, Tasmania, 9–12 February 2021: Geological Society of Australia, p. 45–46.
- Vocale, A 2020, E69/02989 Wineye Project co-funded drilling report for the period 1 January 2020 to 31 December 2020 (R20): Independence Group NL: Geological Survey of Western Australia, Statutory mineral exploration report A124819, 17p.
- Wawryk, MJ and Hancock, EA 2019, Application of rapid benchtop X-ray powder diffractometry for identification and characterization of mineral phases in geological materials: Geological Survey of Western Australia, Record 2019/9, 31p.
- Winter, JD 2010, Principles of igneous and metamorphic petrology (2nd edition): Pearson, London, UK, 739p.

RECORD 2022/11

PORTABLE XRF ANALYSIS IN THE JOE LORD AND PERTH CORE LIBRARIES – METHODOLOGY AND CASE STUDIES

MJ Wawryk and EA Hancock

Access GSWA products



All products

All GSWA products are free to download as PDFs from the DMIRS eBookshop <www.dmirs.wa.gov.au/ebookshop>. View other geoscience information on our website <www.dmirs.wa.gov.au/gswa>.



Hard copies

Limited products are available to purchase as hard copies from the First Floor counter at Mineral House or via the DMIRS eBookshop <www.dmirs.wa.gov.au/ebookshop>.



Fieldnotes

Fieldnotes is a free digital-only quarterly newsletter which provides regular updates to the State's exploration industry and geoscientists about GSWA's latest programs, products and services. Access by subscribing to the GSWA eNewsletter <www.dmirs.wa.gov.au/gswaenewsletter> or downloading the free PDF from the DMIRS eBookshop <www.dmirs.wa.gov.au/ebookshop>.



GSWA eNewsletter

The GSWA eNewsletter is an online newsletter that contains information on workshops, field trips, training and other events. To keep informed, please subscribe <www.dmirs.wa.gov.au/gswaenewsletter>.



Further details of geoscience products are available from:

First Floor Counter
Department of Mines, Industry Regulation and Safety
100 Plain Street
EAST PERTH WESTERN AUSTRALIA 6004
Phone: +61 8 9222 3459 Email: publications@dmirs.wa.gov.au
www.dmirs.wa.gov.au/GSWApublications